São Paulo, December, 2015.

ACP

Dear Sirs,

The manuscript “Impact of vehicular emissions on the formation of fine particles in the Sao Paulo Metropolitan Area: A numerical study with the WRF-Chem model” was first submitted on 23 Jan 2015. The reviewers pointed out many important questions during the time it was open for suggestions and comments. We tried to answer all the questions and the manuscript was re-written and re-submitted. We would like to thank the reviewers for the comments as this version was improved substantially. We try to answer the last questions that were presented by the reviewers. Regarding some specific comments of the reviewers:

The reviewer suggested the presentation of the model evaluation by the analysis of a base case simulation. This was done with the inclusion in the analysis of more statistical index to evaluate the model performance: in addition to the correlation coefficient (R), mean bias (MB), root mean square error UB ($RMSE_{UB}$), it was calculated the mean fractional bias (MFB) and mean fractional error (MFE). The comparisons between simulated and measured parameters for different air quality stations as well as additional tables and figures related to these comparisons are presented in the supplementary material. The simulations for wind, temperature, humidity and air quality parameters are compared to the measured data.

Another important point that is discussed by the reviewer is the consideration in the modelling of only the mobile sources. It is an important point that is more discussed in this new version of the manuscript. We totally agree that a base case simulation should include all possible emissions sources. It is, however, worthwhile to mention that in southeastern Brazil's metropolitan areas, mainly in the São Paulo Metropolitan Area (SPMA), most of the energy is used by the transportation sector. According to official emission inventory provided by the Sao Paulo State Environmental Agency (CETESB, 2013) 80% of NOx, 97% of CO, and 87% of VOC are emitted by the vehicular fleet, being most of NOx associated to diesel combustion and most of CO and VOC from gasohol and ethanol combustion (CETESB, 2013). Previous studies applying Receptor Models to trace-elements, performed by the Laboratório de Análise dos Processos Atmosféricos (LAPAt) of the Atmospheric Sciences Department, showed that only 13% of the fine particles mass (PM2.5) in São Paulo is associated to the emission by the industrial process (oil burning and secondary aerosol) (Andrade et al., 2012). The fine particles are composed mostly by carbonaceous aerosols, 60% organic compounds and 20% Black Carbon according to studies performed in São Paulo in tunnels measurements described by (Brito et al., 2013; Pérez-Martínez et al., 2014). In addition, it is also important to remind that the present study focuses especially on the potential formation of secondary particles from the primary emission of gases coming from on-road vehicles (the Guenther biogenic emissions module was chosen to minimize the impact of vegetation). For these reasons, we suggest that the consideration of two simulation scenarios: the first, a base case simulation (Case_0) including emissions of gases and aerosols from nature and on-road vehicles; and the second (Case_1) seems to the first but with no aerosol particles emission, could be a direct and suitable way to

assess the impact of vehicular emissions on the potential formation of secondary aerosols.

References

Andrade, M. F., Fornaro, A., Miranda, R. M., Kerr, A., Oyama, B., Andre, P. A., and Saldiva, P.: Vehicle emissions and PM2.5 mass concentration in six Brazilian cities, Air Quality, Atmosphere and Health, 5, 79-88, 2012.

Brito, J., Rizzo, L. V., Herckes, P., Vasconcellos, P. C., Caumo, S. E. S., Fornaro, A., Ynoue, R. Y., Artaxo, P., and Andrade, M. F.: Physical-chemical characterisation of the particulate matter inside two road tunnels in the Sao Paulo Metropolitan Area, Atmos. Chem. Phys., 13, 12199-12213, 2013.

CETESB-Companhia de Tecnologia de Saneamento Ambiental. Relatorio Anual de Qualidade do Ar do Estado de Sao Paulo 2012, Sao Paulo, 2013.

Pérez-Martínez, P. J., Miranda, R. M., Nogueira, T., Guardani, M. L., Fornaro, A., Ynoue, R., and Andrade, M. F.: Emission factors of air pollutants from vehicles measured inside road tunnels in Sao Paulo: case study comparison, Int. J. Environ. Sci. Technol., 11, 2155-2168, 2014.

Impact of vehicular emissions on the formation of fine particles in the Sao Paulo Metropolitan Area: A numerical study with the WRF-Chem model

Angel Vara-Vela[1], M. F. Andrade[1], Prashant Kumar[2,3], R. Y. Ynoue[1], and A. G. Muñoz[4,5]

[1]Department of Atmospheric Sciences, Institute of Astronomy, Geophysics and Atmospheric Sciences, University of Sao Paulo, Sao Paulo, Brazil

[2]Department of Civil and Environmental Engineering, Faculty of Engineering and Physical Sciences (FEPS), University of Surrey, Guilford GU2 7XH, United Kingdom

[3]Environmental Flow (EnFlo) Research Centre, Faculty of Engineering and Physical Sciences, University of Surrey, Guildford GU2 7XH, United Kingdom

[4]International Research Institute for Climate and Society (IRI), The Earth Institute, Columbia University, NY, USA

[5]Centro de Modelado Científico (CMC), Universidad del Zulia, Maracaibo, Venezuela

Corresponding author: A. V. Vela (angel.vela@iag.usp.br)

Abstract

The objective of this work is to evaluate the impact of vehicular emissions on the formation of fine particles ($PM_{2.5}$; ≤2.5 μm in diameter) in the Sao Paulo Metropolitan Area (SPMA) in Brazil, where ethanol is used intensively as a fuel in road vehicles. The Weather Research and Forecasting with Chemistry (WRF-Chem) model, which simulates feedbacks between meteorological variables and chemical species, is used as photochemical modelling tool to describe the physico-chemical processes leading to

evolution of number and mass size distribution of particles through gas-to-particle conversion. A vehicular emission model based on statistical information of vehicular activity is applied to simulate vehicular emissions over the studied area. The simulation has been performed for a one month period (7 August - 6 September 2012) to cover the availability of experimental data from the NUANCE-SPS (Narrowing the Uncertainties on Aerosol and Climate Changes in Sao Paulo State) project that aims to characterize emissions of atmospheric aerosols in the SPMA. The availability of experimental measurements of atmospheric aerosols and the application of the WRF-Chem model made it possible to represent some of the most important properties of fine particles in the SPMA such as the mass size distribution and chemical composition, besides allowing us to evaluate its formation potential through the gas-to-particle conversion processes. Results show that the emission of primary gases, mostly from vehicles, led to a production of secondary particles between 20 and 30 % in relation to the total mass concentration of $PM_{2.5}$ in the downtown SPMA. Each of $PM_{2.5}$ and primary natural aerosol (dust and sea salt) contributed with 40-50% of the total PM_{10} (i.e. those $\leq$10 μm in diameter) concentration. Over 40% of the formation of fine particles, by mass, was due to the emission of hydrocarbons, mainly aromatics. Furthermore, an increase in the number of small particles impaired the ultraviolet radiation and induced a decrease in ozone formation. The ground level O_3 concentration decreased by about 2% when the aerosol-radiation feedback is taken into account.

1. Introduction

The Sao Paulo Metropolitan Area (SPMA), in the southeast region of Brazil, is considered a megalopolis comprised of Sao Paulo city and more 38 municipalities. One of the main concern in the SPMA is the occurrence of violations of air quality standards

for ozone and fine particles at different air quality stations from the Sao Paulo Environmental Agency (CETESB). The air pollutant emissions in the SPMA are related to the burning of the fuels: ethanol, gasohol (gasoline with 25% ethanol) and diesel. Recent work of Carvalho et al. (2014) reported a substantial increase in number of road vehicles from 1 million in 2000 to almost 7 million in 2014, together with an overview of the pollutants concentration, fuel use in the SPMA and the relationship between the emissions and the improvement in the air quality in past years.

They constitute the main cause of impairment to air quality in the SPMA, but the number of air quality standard violations has decreased for almost all pollutants with the exception of $PM_{2.5}$ and O_3. Both these pollutants are impacted by the vehicular emissions and have experienced an increase in the number of violations of local air quality standards as discussed in detail by Carvalho et al. (2014). Pérez-Martínez et al. (2015) have analyzed the monthly mean values for the regulated pollutants from 2000 to 2013 for the air quality stations in the SPMA. They found a decrease in the average concentration of NOx, CO and PM_{10} by 0.65, 0.37 and 0.71 % $month^{-1}$, respectively, although the sales of the fuels (gasoline, ethanol, and diesel) had increased by 0.26, 1.96 and 0.38 % $month^{-1}$, respectively.

A recent report from CETESB (CETESB, 2013) highlighted that, in 2012, the vehicles contributed with about 40% of the total PM_{10} mass concentrations through direct emissions. If we consider the secondary aerosols, which were about 25% of PM_{10} as estimated by CETESB (2013), these were mainly found to be formed by chemical reactions between gases released from exhaust of vehicles.

The implementation of the Program for the Control of Vehicular Emission (PROCONVE) established by the Brazilian Government in the 80's, enforcing measures such as use of catalytic converters and ethanol as additive to gasoline in substitution of

tetraethyllead, led to decrease in emissions of CO and VOCs and hence their ambient concentration. Although the emissions have been controlled by regulations, the number of vehicles has increased substantially and faster than the replacement of the old vehicles by the new ones (Pérez-Martínez et al., 2014). According to CETESB (2013), the road vehicles contributed up to about 97, 87 and 80% of CO, VOCs and NOx emissions in 2012, respectively, being most of NOx associated to diesel combustion and most of CO and VOCs from gasohol and ethanol combustion. Receptor modelling studies applied to six capital cities in Brazil (Andrade et al., 2012) showed that only 13% of $PM_{2.5}$ in the SPMA is associated to the emission by the industrial processes (oil burning and secondary aerosols).

[a1] Comentário: Added.

To date, many studies assessing the impact of biofuels on the air quality have been performed in Brazil. For example, Anderson (2009) conducted a review concerning the use of ethanol fuel in Brazil. His work highlighted that the atmospheric concentrations of acetaldehyde and ethanol are much higher in Brazil in comparison with the other areas of the world. Costa and Sodré (2010) showed that exhaust emissions of hydrous ethanol reduced CO and Hydrocarbons (HC), but increased CO_2 and NOx levels.

A number of past studies has shown the significant participation of the carbonaceous compounds in the concentration of fine particles in the SPMA (Albuquerque et al., 2011; Miranda and Andrade, 2005; Ynoue and Andrade, 2004; Castanho and Artaxo, 2001). Studies conducted on ambient air pollution in the SPMA have also shown that BC explains 21% of mass concentrations of fine particles ($PM_{2.5}$; ≤2.5 μm in diameter) compared with 40% of organic carbon (OC), 20% of sulfates, and 12% of soil dust (Andrade et al., 2012). Most of the observed ambient $PM_{2.5}$ mass concentration usually originates from precursors gases such as sulphur dioxide (SO_2),

ammonia (NH_3), nitrogen oxides (NOx) and volatile organic compounds (VOCs) as well as through the physico-chemical processes such as the oxidation of low volatile hydrocarbons noted above transferring to the condensed phase (McMurry et al., 2004; Heal et al., 2012). Since these processes are often photo-chemically driven, the resultant aerosol usually falls into the category of secondary photochemical pollutant (Jenkin and Clemitshaw, 2000). Oxidation of VOCs can produce species of sufficiently low vapor pressure to be condensable, leading to the formation of secondary organic aerosol (SOA) (Kroll and Seinfeld, 2008). Fine particles in SPMA have a great participation on its composition of SOA, formed from the emissions of VOCs, which have the same origin of the primary compounds involved in the formation of ozone, from the burning of fuels. The participation of the biogenic emission is considered to be small in the formation of particles in the metropolitan area of the city according to previous studies of Martins et al. (2006).

The impact of the fine particles has been discussed in previous works, with evaluation of the scattering and absorbing effects of the aerosol (e.g. Li et al., 2005; Real et al., 2011). Vehicular emissions of particulate matter (PM) in the SPMA have a high percentage of BC (Brito et al., 2013), which after emitted to the atmosphere can enhance the absorption coefficient and thus the attenuation rates.

One of the most important aspects of this work is the quantitative analysis of the formation of $PM_{2.5}$ and ozone (O_3) in the SPMA. Photolysis of O_3 by ultraviolet light in the presence of water vapor is the main source of hydroxyl radical (OH), the most important radical in the atmosphere in terms of reactivity (Monks, 2004). At the same time, OH levels in the atmosphere directly determine the oxidation rate of the precursors of secondary aerosols. Oxidation products of VOCs and semi-VOCs by OH are the most important precursors of SOA (Li et al., 2011a). Although VOCs and NOx are

126 precursors of both O_3 and a fraction of atmospheric PM (NO_3^- and secondary organics)
127 while they influence indirectly the formation of the rest of the secondary PM
128 components like $SO_4^=$, their control strategies that are optimal for O_3 controls may even
129 increase $PM_{2.5}$ concentrations (McMurry et al., 2004). Such an analysis is important to
130 evaluate the contribution of the vehicular fleet using different kind of fuels to the
131 concentration of fine particles. In this sense, a numerical study with an adequate
132 physical approach, representing particles in the modelling system, is important to
133 understand the formation of secondary aerosols from primary emission of gases in a
134 metropolitan area where the composition of fuel in vehicular fleet has changed
135 significantly over the past years. Therefore, the goal of the present study is to evaluate
136 the impact of vehicular emissions on the formation of fine particles in the SPMA,
137 focusing especially on the potential formation of secondary particles from the primary
138 emission of gases coming from on-road vehicles. The impact of aerosol particles on the
139 ozone photochemistry is also examined by means of numerical simulations.
140 Measurements were performed to provide input data to evaluate the modelling
141 performance and estimate the vehicular emission factors. Aerosol measurements were
142 taken from field campaigns that were carried out as part of the Narrowing the
143 Uncertainties on Aerosol and Climate Changes in Sao Paulo State (NUANCE-SPS)
144 project (http://nuance-lapat.iag.usp.br/). These campaigns took place between July and
145 September 2012. An online-coupled meteorology and chemistry model, i.e., the
146 Weather Research and Forecasting with Chemistry (WRF-Chem) model, has been used
147 to characterize and describe the physico-chemical processes involved in both the
148 formation and growth of new particles over the SPMA in southern Brazil. The details of
149 the experimental campaigns, WRF-Chem model and emissions are described in Section

2. Results from modelling experiments and comparison with measurements are presented in Section 3. Finally, the summary and conclusions are given in Section 4.

2. Methodology

2.1. Observational datasets

The study period starting from 7 August until 6 September 2012 was selected for comparison with the modelled results (Section 2.2) due to the availability of experimental data from the NUANCE-SPS project. The aim of NUANCE-SPS was to evaluate the impact of emissions in the SPMA on the air quality and changing climatic conditions, and feedback mechanisms between climatic perturbations produced by both primary and secondary emissions and urban atmospheric processes. Aerosol observation datasets used in this work were collected using a Dichotomous sampler (Wedding et al., 1980) and a Micro-Orifice Uniform Deposit Impactor (MOUDI, model 100; MSP Corporation - Marple et al., 1986). The MOUDI impactor collected particles in 10 size classes with nominal 50% cut-off diameters: 10, 5.6, 3.2, 1.8, 1.0, 0.56, 0.32, 0.18, 0.1 and 0.06 μm. Particles smaller than 0.06 μm were collected in a subsequent stage or after-filter. The samples collected with the MOUDI impactor were deposited on a polycarbonate membrane filter with 0.4 μm porous and for the Dichotomous sampler the substrate was a teflon membrane filter with 2 μm porous. The after-filter in the MOUDI impactor is a 33 mm teflon membrane filter, which was not submitted to the reflectance analysis. The collected membrane filters sampled with the Dichotomous and MOUDI samplers were analyzed to the identification of trace elements of mass through X-ray diffraction analysis, mass concentration through gravimetric analysis, and black and organic carbon through reflectance and thermo analysis using a thermal-optical transmittance (TOT) (Sunset Laboratory Inc. – Birch and Cary, 1996). Ion

concentrations were evaluated through the ion chromatography analysis of the soluble material collected on the membrane filters (sulphate, nitrate, ammonium, sodium, and chloride). All these samplings were performed on the roof of the main building of the Institute of Astronomy, Geophysics and Atmospheric Sciences of the University of Sao Paulo (IAG-USP) (hereafter also referred as IAG-USP measurement site or simply IAG-USP), which is inside a small green-park (approximately 7.4 km^2), with local traffic during the day and surrounded by major roads with intense traffic by light and heavy-duty vehicles (Nogueira et al., 2014). Table 1 lists the aerosol instrumentation deployed roughly at the IAG-USP measurement site. In addition, ambient data from the CETESB's air quality monitoring network and the IAG-USP's climatological station (hereafter also referred as AF-IAG) were also considered for evaluation of numerical simulations. The locations of measurement sites are depicted in Fig. 1 whereas geographic coordinates, urban-suburban classification, and the list of pollutants and meteorological parameters monitored at each site is available in Table 2.

[a2] Comentário: Added.

2.2. WRF-Chem model

The WRF-Chem model is a fully coupled online meteorological and chemical transport model (Grell et al., 2005), supported by National Center for Atmospheric Research (NCAR) of the USA and several other research institutions around the world. This model is a system of two key components. The WRF-Chem meteorological component, the Weather Research and Forecasting (WRF), is a system configured for both research and operational applications. The dynamical core used in this study is the Advanced Research WRF (ARW). Model's equations into ARW are solved to non-hydrostatic conditions on a fully compressible atmosphere. Further details on the modelling system can be found on the WRF model website (http://www.wrf-

model.org). On the other hand, the WRF-Chem chemical component treats chemical processes such as dry deposition, gas-phase chemistry, photolysis rates, and aerosols chemistry. A detailed description of the WRF-Chem model can be found on its website (http://ruc.noaa.gov/wrf/WG11). Since both meteorological and chemical components are fully coupled, the transport of all chemical species is on-line. The gas-phase chemistry and aerosol modules employed in this study are the Regional Acid Deposition Model, version 2 (RADM2) (Chang et al., 1989) and the Modal Aerosol Dynamics Model for Europe - Secondary Organic Aerosol Model (MADE - SORGAM) (Ackermann et al., 1998; Schell et al., 2001), respectively. The inorganic species included in the RADM2 mechanism are 14 stable species, 4 reactive intermediates, and 3 abundant stable species (oxygen, nitrogen and water). Atmospheric organic chemistry is represented by 26 stable species and 16 peroxy radicals. The RADM2 mechanism represents organic chemistry through a reactivity aggregated molecular approach (Middleton et al., 1990). Similar organic compounds are grouped together in a limited number of model groups through the use of reactivity weighting. The aggregation factors for the most emitted VOCs are given in Middleton et al. (1990).

On the other hand, the most important process for the formation of secondary aerosol particles is the homogeneous nucleation in the sulfuric acid-water system. It is parameterized in MADE, following the method of Kulmala et al. (1998). Aerosol growth by condensation occurs in two steps: the production of condensable material (vapor) by the reaction of chemical precursors, and the condensation and evaporation of ambient volatile species on aerosols. The inorganic chemistry system, based on the Model for an Aerosol Reacting System (MARS) (Saxena et al., 1986) and its modifications by Binkowski and Shankar (1995), calculates the chemical composition of a sulphate-nitrate-ammonium-water aerosol according to equilibrium

thermodynamics. The organic aerosol chemistry is based on the SORGAM, which assumes that SOA compounds interact and form a quasi-ideal solution (Grell et al., 2005). The SOA formation in SORGAM follows the two-product approach (Odum et al., 1996) where the oxidation of hydrocarbons produces two types of modelled semivolatile compounds that are partitioned between the gas and particle phases after considering the absorptive partitioning theory (Pankow, 1994a; b). The primary organic aerosol (POA) in MADE is calculated from the primary anthropogenic emission of OC. Then, one may calculate the predicted OC concentration from the sum of both SOA and POA. The concurrent organic matter (OM) can be obtained from the OC concentration by application of a conversion factor. Brown et al. (2013) showed that the average OM:OC ratio was 1.54 (with a standard deviation of 0.2) for sites with low amount of secondary aerosol formation. It is important to note that this ratio can change from one place to another. In areas impacted by biomass burning the ratio can be higher. Gorin et al. (2006) assumed a ratio of 1.6 for the conversion from OC to OM over an area that experiences a significant wood smoke influence.

2.2.1. Model configuration

WRF-Chem version 3.5 was configured with three nested grid cells: coarse (75 km), intermediate (15 km) and fine (3 km). The coarse grid cell covered a big region of Brazil and also of the Atlantic Ocean. The intermediate grid covered the southeast Brazil while the fine grid cell covered barely the SPMA and metropolitan areas nearest to it. Fig. 1 shows the arrangement of measurement sites and topography in the downtown area of the 3-km modelling domain. The initial and boundary meteorological conditions are from the National Center for Environmental Prediction's Final Operational Global Analysis with 1^{o} of grid spacing, 26 vertical levels and are available

every six hours: 00, 06, 12 and 18 UTC (http://rda.ucar.edu/datasets/ds083.2/). The initial and boundary chemical conditions for representing gases and aerosols background concentration were obtained from the Model for Ozone and Related chemical Tracers, version 4 (MOZART-4; Emmons et al., 2010). This model was driven by meteorological inputs from the Goddard Earth Observing System Model, version 5 at a horizontal resolution of $1.9^{o}\times2.5^{o}$, 56 vertical levels that are also available every six hours. Table 3 lists the WRF-Chem configuration options employed by this study.

WRF-Chem simulation with coupled primary aerosol (dust, sea salt and anthropogenic) and gas (biogenic and anthropogenic) emission modules, together with the direct effect of aerosol particles turned on, is performed as the control simulation in order to evaluate the model performance (hereafter referred to as Case_0). For secondary aerosols, a simulation scenario (Case_1) with biogenic and anthropogenic gases emission is performed to evaluate its formation potential. An additional simulation (Case_2) is also performed to evaluate the impact of aerosols on ozone photochemistry. Notation and description of simulations are listed in Table 4. The first seven days of each simulation were not analyzed and used for model spin-up.

2.3. Emissions

2.3.1. Anthropogenic emissions

Because on-road vehicles are the most important sources of air pollution in southeast Brazil's metropolitan areas, particularly in SPMA where, according to CETESB, more than 80% of pollutant emissions are generated by vehicular emissions; the anthropogenic emissions of trace gases and particles in both 3 and 15 km modelling domains were considered to include emissions only coming from on-road vehicles

[a3] Comentário: Added.

through the use of a vehicular emission model developed by the IAG-USP's Laboratory of Atmospheric Processes (LAPAt). Basically, this model considers the number of vehicles, vehicular emission factors, and average driving kilometers for vehicle per day as basic parameters for the calculation of exhaust emissions considering different vehicle types (light-duty vehicles, heavy-duty vehicles, and motorcycles) and different fuel types (ethanol, gasohol, combination of any proportion of gasohol and ethanol, and diesel) according to CETESB (2012). The details of this model are available in Andrade et al. (2015). In the case of VOCs, there are other two relevant emissions (fuel transfer and evaporative processes) associated with the vehicles, besides the exhaust emissions. Because of the complexities in the spatial representation due to a numerous factors such as emissions at service stations, such emission sources are assumed to be emitted by exhaust of vehicles for the sake of simplicity. The vehicular fleet and intensity of use datasets are provided by the National Department of Traffic (DENATRAN) and the Sao Paulo Transporte (SPTrans), respectively. Emission factors for road vehicles for most pollutants were considered from previous studies performed inside road tunnels (i.e. Janio Quadros, referred as JQ tunnel, and the tunnel 3 of the Rodoanel Mario Covas that is referred hereafter as RA tunnel) located within the SPMA (Pérez-Martínez et al., 2014; Nogueira et al., 2014). However, emission factors for VOCs are considered from dynamometer protocols (CETESB, 2010). VOCs and PM speciation profiles used by gas-phase and aerosol chemical modules were also obtained from NUANCE-SPS experimental campaigns performed in 2011 (tunnel measurements) and 2012 (ambient data). It is important to note that due to the lack of information on vehicular emission factors and intensity of use for most of the other metropolitan areas inside both modelling domains (e.g. the Campinas Metropolitan Area, which is shown by the second largest grey stain in Fig. 2), the calculation of vehicular emissions for these

urban areas was carried out on the basis of the parameters found for the SPMA. The number of vehicles in any modelling domain is calculated from the sum of the number of vehicles in each one of the main urban areas inside the modelling domain in question.

Spatial distribution of emissions for the 3 km modelling domain resolution was based on road density products compiled by the OpenStreetMap project and extracted from the Geofabrik's free download server (http://download.geofabrik.de). Urban areas were assumed to allocate high emissions since these concentrate a road density greater than other areas. In the case of the 15 km modelling domain, emissions are based on night-time lights data from the Defense Meteorological Satellite Program (http://ngdc.noaa.gov/eog/dmsp/downloadV4composites.html). These images are 30 arc second grids, spanning from -180^{o} to $+180^{o}$ longitude and -65^{o} to $+75^{o}$ latitude and contain the lights from cities, towns and other sites with persistent lighting, including gas flares. Cleaned up night-time light points with no ephemeral events such as forest fires are used to allocate emissions. To estimate the number of vehicles in each grid point of both domains, the sum of individual intensities at each point (i.e. total road length for the 3 km modelling domain and night-time light for the 15 km modelling domain) is firstly normalized by the total fleet, and then distributed uniformly using the total fleet distribution so that emissions in urban areas are mainly represented by emissions coming from their vehicles. Furthermore, due to the complexity involved in describing the temporal variation of emissions at each grid point, median values for vehicular traffic obtained from measurements inside the JQ and RA tunnels (Pérez-Martínez et al., 2014) were used for distributing the emissions during the day in both domains. This approximation followed the approach used by Fast et al. (2006) where emission profiles were calculated from median diurnal variations on weekdays and weekends. We have applied the same constant diurnal cycle at all grid points where

emissions have values greater than zero. VOC and PM emission profiles were assumed to be the same as for CO and NOx emission profiles since these pollutants are also characteristic tracers of emissions of light-duty and heavy-duty vehicles, respectively. Fig. 2 shows the maximum hourly emission rates for aromatic VOCs in the 3 km modelling domain. Anthropogenic emissions were not considered in the 75 km modelling domain.

The Another Assimilation System for WRF-Chem (AAS4WRF) chemical emissions pre-processor developed by the Latin American Observatory (OLE2; Muñoz et al., 2010; 2012) was used to scale emission rates on WRF curvilinear coordinates. AAS4WRF is appropriate to write chemical emission rates from both surface and elevated sources in the proper WRF data file format, providing an alternative tailored way to assimilate emissions to WRF-Chem. The method is explained in the OLE2 Wiki pages in detail (http://www.cmc.org.ve/mediawiki/index.php?title=Calidad_de_Aire).

2.3.2. Other emissions

Biogenic emissions are calculated online based on the Guenther scheme (Guenther et al., 1993; 1994). The Guenther biogenic emissions model calculates the emission rates using temperature, photo-synthetically active radiation flux and land-use data as the U.S. Geological Survey (USGS) land-use cover system classification if coupled with the WRF model. However, as indicated in the WRF-Chem emissions guide (http://ruc.noaa.gov/wrf/WG11/Emission_guide.pdf), several key chemical species would have been representing relatively low emission rates because of the limited vegetation types in the simulation, and thus their impacts are anticipated to be much lower than those from vehicular emissions.

Dust and sea salt emissions are calculated online following the works of Ginoux et al. (2001) and Gong (2003), respectively. The calculation of Ginoux et al. (2001) for the uplifting of dust particles is based on the surface wind speed, wetness and information on soil characteristics. The model then solves the continuity equation including the emission, chemistry, advection, convection, diffusion, dry deposition, and wet deposition of each species. The parameterization of sea salt aerosol source function of Gong (2003) is an extended parameterization of Monahan et al. (1986), which scales the generation of marine aerosols from mechanical disruption of wave crests by the wind and sea surface covered by whitecaps.

3. Results and discussion

3.1. Characterization of meteorological conditions

In order to study and understand the spatial and temporal variability of atmospheric aerosols, O_3, and other pollutants (i.e. CO, NOx) during the study period, it was first necessary to analyze the behavior of main meteorological systems acting on the atmospheric environment of the SPMA and surrounding areas.

According to the monthly climate reports from the IAG-USP's Climate Research Group (GrEC), the observed precipitation rates were lower than the climatological value in SPMA (anomaly of -38.6 mm) and larger part of the Sao Paulo State during August 2012. Negative anomalies on the precipitation were caused by the intensification of the South Atlantic Subtropical High (SASH). These conditions established an easterly wind anomaly pattern at the 850 hPa level. Conditions were unfavorable for relative humidity coming from the Amazon due to the Low Level Jet (LLJ) and less intense Alisian winds in the Tropical Atlantic (GrEC, 2012a). However, the action of frontal systems favored the rain accumulation in September 2012, mainly in western Sao Paulo State where the

374 greater positive amount of anomalies was observed. Precipitation events were
375 predominantly observed during the second half of the month. In this case, the wind
376 pattern showed an opposite configuration to that observed in August 2012 as a result of
377 the weakening of the SASH (GrEC, 2012b). The IAG-USP's climatological station
378 recorded an accumulated precipitation of about 1.3 mm on three days of occurrence (28
379 August, 30 August and 4 September 2012) and an easterly wind pattern with a median
380 intensity of 2 m s^{-1} during the period between 07 August and 06 September 2012. Fig. 3
381 shows the hourly accumulated precipitation and relative humidity observed at the IAG-
382 USP's climatological station.

383

384 **3.2. Analysis of aerosol species**

385 Aerosol analysis included species such as organic carbon (OC), elemental
386 carbon (EC), sulphate, nitrate, ammonium, sodium and chloride in addition to other
387 elemental constituent of PM. All the samplings for these species were performed at
388 IAG-USP. Results showed that the major contributors to the concentration of fine
389 particles are OM (55.7%; OM:OC ratio of 1.5 found by Brito et al. (2013)) and EC
390 (15%), followed by sulphate (2.9%), ammonium (2.1%), sodium (1.9%), nitrate (0.5%)
391 and chloride (0.3%). The remaining mass (21.6%) is calculated by determining of the
392 difference between the total mass of $PM_{2.5}$ (from the gravimetric analysis) and the sum
393 of the masses of 7 individual compounds, as noted above. Part of this remaining mass is
394 related to the water content of aerosols (Andrade et al., 2012).

395 On the other hand, $PM_{2.5}$, PM_{10} and size distribution of particles measured at
396 IAG-USP show that the study period was characterized by a reduction in the

concentrations up to the end of August 2012 when their minimum values were achieved. This reduction was related to the action of a semi-stationary front between the coasts of Sao Paulo and Parana States. After the passage of this system, aerosol concentrations have significantly increased what could be related to an increase in relative humidity once the SASH system is moved away from the continent, as well as the transport of aerosol particles produced by forest fires in the central-west region of Brazil and the Sao Paulo State. Several studies have shown the contribution of forest fires on the atmospheric aerosol concentrations in SPMA (Vieira-Filho et al., 2013; Vasconcellos et al., 2010). One way to qualitatively evaluate the contribution of forest fires on aerosol concentrations is by using the air mass trajectories. The Hybrid Single-Particle Lagrangian Integrated Trajectory (HYSPLIT) model (Draxler and Hess, 1998) was used to calculate backward trajectories of air masses in order to identify atmospheric transport of air mass from forest fire areas. Fig. 4 shows the three-day backward trajectories of air masses starting at IAG-USP for the days 9 and 31 August and 5 September, when increases in the OC and EC concentrations were observed at IAG-USP. The pink markers on the map represent the observed fire locations during the study period considering different satellite products (GOES, AQUA, TERRA, NOAA).

Fig. 5 shows the concentration of OC, EC and some species of $PM_{2.5}$ during the study period at IAG-USP. We can observe eleven exceedances of $PM_{2.5}$ concentration with respect to the air quality standard of 25 μg m^{-3} (see grey line in Fig. 5a) established by the World Health Organization (WHO). These exceedances have mainly occurred at the beginning and at the end of the study period when an increase in the concentrations of OC and EC were observed. The increasing organic matter could be associated to traffic incidents which may raise the emissions, which in case of less favorable meteorological conditions (e.g. lower height of lower planetary boundary layer, PBL, or

slow transport of air pollutants) may have led to a more efficient formation of secondary particles. Castanho and Artaxo (2001) analyzed the behavior of the aerosol composition in SPMA and showed the increase in the concentration of inorganic and organic material in the winter season compared to the summer season, explaining this behavior with the meteorological characteristics: dry conditions with low height inversion layer in the wintertime and a rainy summer.

Size distributions of aerosol mass indicate that the majority of sulphate, ammonium and PM_{10} mass concentration is distributed in the size range with diameters between 0.1 and 1 µm, commonly known as accumulation mode particles (Kumar et al., 2010). In the cases of nitrate, sodium, and chloride, most part of mass was concentrated in particles with diameters greater than 1 µm.

3.3. Comparison of baseline simulation with observations

All the numerical results presented in this section, for the purpose of comparison with the measurements, were obtained from the baseline simulation (Case_0). The predicted temperature, humidity, and 10-m wind speed and direction have been compared to measurements from the AF-IAG and INT measurement sites. Overall, the model captured the diurnal variation of temperature, relative humidity, and wind directions reasonably well. However, the predicted wind speeds were higher than the observed values. To evaluate the model performance in solving the meteorology and chemical species, we computed the statistics correlation coefficient (R), mean bias (MB), mean fractional bias (MFB), mean fractional error (MFE), and root mean square error UB ($RMSE_{UB}$). The definitions of these statistics are given in the Appendix. Fig. 6 shows the predicted average of 10-m wind vectors and 2-m temperature for the whole study period in the 3 km modelling domain. Blue dots represent the locations of AF-

[a4] Comentário: Added.

IAG and INT sites, while the numbers in cyan indicate the observed average temperatures (i.e. 17.7 °C at AF-IAG and 17.8 °C at INT). On an average, the predicted wind direction was easterly in SPMA, which has somewhat affected the spatial distribution of aerosol particles as examined later in this section. Likewise, the statistics used to quantify the model performance in the representation of PM concentration show that, in general, most of prediction-observation pairs present good correlation coefficients, mainly those for PM_{10}, but with negative biases and standard deviations lower than those for observations (see Fig. 10). Table 5 summarizes the performance statistics used in this study showing comparisons between WRF-Chem predictions and observations. The evaluation of WRF-Chem predictions for meteorology and chemical species on a site-by-site basis is presented in the sections 1 and 2, respectively, of the supplementary material. Figs. 7, 8 and 9 show the observed and predicted temporal variations of $PM_{2.5}$, PM_{10} and O_3 concentrations at 3, 10 and 6 sites in the SPMA, respectively, with some measurement sites sharing the same grid point for comparisons due to the geographical proximity (e.g. the sites IAG-USP and IPEN-USP both separated around 900 m from each other). These figures suggest that predicted concentrations did not present any significant spatial variation in the downtown SPMA and were generally underestimated when compared to measurements. This under prediction could be associated with an underestimation on the vehicular emissions as well as other emission sources (e.g. emissions coming from industry) that are disregarded in this study, in addition to predicted surface winds more intense than those observed, leading to a dilution of aerosol particles in the SPMA. The high concentrations of $PM_{2.5}$ and PM_{10} observed at the beginning and at the end of the study period, whose variability and trends were reasonably well captured by the model, could be related with the emission of high aerosol loadings due to traffic incidents as well as

[a5] Comentário: Modified. Also, the Taylor reference was moved to the figure caption of Figure 10.

[a6] Comentário: Modified and relocated.

[a7] Comentário: Added.

[a8] Comentário: Added.

472 the establishment of lower PBL heights, commonly observed under post-frontal
473 situations. The results for this simulation (Case_0) show that overall the predicted PBL
474 heights (not shown here) have a regular diurnal variation in the downtown SPMA with
475 averaged daily values around 500 m at both the beginning and the end, and of up to 700
476 m in the middle of the study period, when lower concentrations of aerosols were
477 observed.

478 Figures 11-13 show the predicted average surface distribution of $PM_{2.5}$, PM_{10}
479 and $PM_{2.5}$:PM_{10} ratio for the 3 km modelling domain, respectively. Red dots and cyan
480 numbers represent the locations and the observed mean PM concentrations (or mean
481 PM concentration ratios) at the measurement sites, respectively. Major contributions of
482 $PM_{2.5}$ on the total PM_{10} concentration were observed mainly over offshore continental
483 areas (see Fig. 13). High $PM_{2.5}$:PM_{10} concentration ratios would be firstly associated
484 with the transportation of fine particles and gases from upwind regions (see Fig. 6),
485 followed by a production of fine particles from biogenic emissions. Additional
486 comparisons between the observed and predicted concentrations of OC and EC at IAG-
487 USP (the only site with measurements of OC and EC) are shown in Fig. 14. As it has
488 been pointed out in the section 2 of the supplementary material, under predicted OC
489 concentrations could be associated, among others (e.g., underestimation of POA
490 emissions, inaccurate meteorological predictions), with an underestimation of SOA,
491 probably due to the absence of oxidation of monoterpenes and a limited treatment of
492 anthropogenic VOCs oxidation in the RADM2 mechanism, as discussed by Tuccella et
493 al. (2012). The SORGAM aerosol module considers the formation of anthropogenic
494 SOAs from the oxidation of alkane, alkene and aromatic VOCs as well as the biogenic
495 SOA formation from the oxidation of alpha-pinene, limonene and isoprene VOCs.
496 Recent studies coupling non-traditional SOA models (volatility basis set approaches) in

[a9] Comentário: Modified.

497 WRF-Chem show improvements in the predicted SOA concentrations, although these
498 are still lower than those observed (e.g. Li et al., 2011b; Ahmadov et al., 2012;
499 Shrivastava et al., 2013).

500 On the other hand, measurements of mass size distribution were also made with
501 a MOUDI impactor at IAG-USP, following the protocol describe in Miranda and
502 Andrade (2005). Constituents of aerosol were subsequently determined by X-Ray
503 fluorescence analysis and ion chromatography analysis. As previously indicated in this
504 section, the main identified species are SO_4, NO_3, NH_4, Na and Cl. The observed
505 average aerosol composition is derived using measurements from both MOUDI
506 impactor and SUNSET analyzer. To perform the comparisons of mass size distribution,
507 we adequately joined the MOUDI bin sizes according to the three modes used by the
508 MADE aerosol module: Aitken (<0.1 μm), accumulation (0.1-1 μm) and coarse (>1
509 μm). The observed and predicted aerosol mass size distributions averaged over the same
510 sampling time period (16 days along the study period) are shown in Fig. 15. Over the
511 downtown SPMA, both the observed and predicted fine particles from accumulation
512 mode account for majority of the total $PM_{2.5}$ mass. Since the formation-growth
513 processes of aerosols in question are explicitly treated in the Aitken and accumulation
514 modes, the predicted concentrations for particles larger than 1 μm are assumed to be
515 zero. In this case, the mass of particles larger than 1 μm is allocated to the PM_{10} aerosol
516 variable (see Fig. 15). The comparison between the observed and predicted average
517 contributions for the main identified aerosol constituents at IAG-USP is shown in Fig.
518 16. Both the observed and predicted OC and EC make up the largest fraction of $PM_{2.5}$
519 mass with contributions of 55 and 40%, respectively. In addition, it was found that the
520 predicted SOA concentrations contribute 17% of the predicted total OC concentration at
521 this measurement site. Various global and regional scale SOA simulations have been

conducted using mass-based yield and partitioning coefficients, but they have underestimated the SOA concentrations by roughly an order of magnitude, especially over urban regions (Matsui et al., 2014). Using the same SOA formation approach employed by this study and a conversion factor of 1.6 to convert the emissions of OC to OM, Tuccella et al. (2012) found simulated SOA:OM ratios in the 5-40% range against the observed range of 50-80%. Although the predicted average $PM_{2.5}$ concentration (14.48 μg m^{-3}) was lower than observed (22.32 μg m^{-3}), the mean aerosol chemical composition was reasonably well represented by the model (see Fig. 16).

3.4. Contribution of dust-sea salt and coarse anthropogenic aerosols to PM concentration

The evaluation of the contribution of dust and sea salt aerosols on PM_{10} concentration is performed from the sum of their concentrations divided by the PM_{10} concentration. The simulated average ratio between dust–sea salt aerosols and the total PM_{10} mass concentration is shown in Fig. 17b. High concentration ratios have been observed over the ocean where sea salt emissions are by far the most important aerosols source. Unlike high concentration ratios over the ocean, lower concentration ratios are observed over the continent far away from the coast. In this region, the main sources of atmospheric aerosols would be the emission of primary biological aerosol, SOA formed from the emission of biogenic volatile organic compounds (BVOCs), and forest fires. However, particles could also be transported from remote areas. In addition, we can also observe that dust and sea salt aerosols have a contribution between 40 and 50% of the total PM_{10} concentration in the downtown SPMA. Furthermore, it is possible to estimate the contribution of all the other PM_{10} (i.e., the coarse anthropogenic aerosol) to the total PM_{10} mass concentration. It may be directly calculated from the model or estimated from the Figs. 13 and 17b once the sum of concentrations of $PM_{2.5}$, dust and sea salt,

and coarse anthropogenic aerosol represents 100% of the total PM_{10} mass concentration. For example, we found that the coarse anthropogenic aerosol represents around 10% of PM_{10} in the downtown SPMA.

3.5. Evaluation of secondary aerosol formation

As described in Section 2.1, aerosol module employed by this study (MADE/SORGAM) includes the homogeneous nucleation in the sulphuric acid-water system. The sulphuric acid is the most significant condensable molecule formed in the atmosphere, which has also been long recognised as the most important molecule from the point of view of the nucleation of new particles (Jenkin and Clemitshaw, 2000; Seinfeld and Pandis, 2006). However, for the SPMA, the importance of SOA formed from the anthropogenic emission of fuel used by the transport sector was noted (Salvo and Geiger, 2014). According to the official emission inventory developed by the Sao Paulo Environmental Protection Agency (CETESB, 2013), the SOA explains 51% of the fine particle mass concentration, with the vehicular emission being its main source. The subsequent growth processes involve aerosol growth by condensation of condensable material onto existing particles, and by coagulation of particles to form larger particles (Kumar et al., 2011; 2014). For example, particles in the accumulation mode emerge through coagulation of particles from the Aitken mode (Kumar et al., 2011). It is important to emphasize that the boundaries were updated with gas and aerosol background concentrations coming from the 15 km modelling domain during the whole simulation period. Thereafter, the impact of vehicular emissions on the formation of fine particles was calculated from the predicted $PM_{2.5}$ concentration considering an emission scenario (Case_1) in which only emission of gases from vehicles and vegetation are taken into account to be emitted to the atmosphere from the surface. The predicted average $PM_{2.5}$ (Case_1):$PM_{2.5}$ (Case_0) ratio is shown in Fig.

17a. A contribution between 20 and 30% in the predicted baseline $PM_{2.5}$ concentration in downtown SPMA is found to correspond to the fine particles formation and transportation processes. Higher concentration ratios over the SPMA surroundings (30-50%) could be associated with more efficient biogenic emissions. Overall, it is observed that the formation efficiency increases towards the northwest from the ocean. Deep red areas in Fig. 17a could also be associated with the transportation of fine particles and gases from other regions, in addition to having a more efficient production of fine particles from biogenic emissions. For example, given the distribution of winds in Fig. 6, the northern boundary could represent the main source of particles and gases over this part of the simulation domain. Additionally, the comparison between the predicted and observed OC and EC concentrations at IAG-USP shown in Fig. 14 includes the Case_1 simulation in which only emission of primary gases is taken into account in the assessment of fine particles formation. The concentration peaks observed at the beginning and at the end of the study period may be associated with the transport of aerosol particles from both biomass and fossil fuel burning areas (see Fig. 4). Considering the Case_1 simulation, we can observe very low concentrations for EC (mean concentration of 0.01 μg m^{-3}), as expected. This is because these particles are not produced by photochemical processes in the atmosphere, but associated mainly with the diesel exhaust.

3.6. Aerosol impact on O_3 photochemistry

Ozone photochemistry production mainly depends on the two key photolysis rates, as shown in Eqs. (1) and (2), i.e., shortwave radiation able to reach the surface to break molecules of O_3 and NO_2.

$$O3 + hv \rightarrow O2 + O(^1D)\ (\lambda < 320\ nm) \quad (1)$$

596 $$NO_2 + hv \rightarrow NO + O(^3P) \ (\lambda < 420 \text{ nm}) \quad (2)$$

597 Therefore, the impact of aerosols on O_3 photochemistry has been evaluated from
598 the impact of aerosols on downward shortwave radiation. Attenuation (scattering and
599 absorption) of downward shortwave radiation by aerosols may substantially modify the
600 photolysis rates, and thereby affecting the ozone photochemistry production.

601 The average percentage change in surface O_3 concentrations at 16:00 h (local
602 time) with and without the aerosol-radiation feedback module turned on are shown Fig.
603 17c. Overall O_3 is destroyed or formed (incoming transport from other regions) in small
604 quantities between -1 and +1% in relation to its total concentration. In addition, it was
605 observed that the surface O_3 concentration decreased by around 2% in the downtown
606 SPMA. Li et al. (2011a) found that the impact of aerosols on O_3 formation in Mexico
607 City was most pronounced in the morning with the O_3 reduction of 5-20%, but the
608 reduction is less than 5% in the afternoon. Low reductions in the O_3 concentration in the
609 downtown SPMA compared to results from other studies may be explained by the lower
610 predicted PM_{10} concentrations, which can lead to a minor attenuation of the incoming
611 solar radiation. Simulated mean downward shortwave fluxes at ground surface (not
612 shown) were up to 5% higher for the Case_2 than for the Case_0 during the afternoon.
613 The inclusion of the direct effect of aerosol particles was found to have small reductions
614 in the surface temperature (changes by around 2%), presumably due to an increase in
615 the number of atmospheric processes involving downward longwave fluxes over this
616 area. Forkel et al. (2012) found an underestimation of predicted downward longwave
617 radiation over the southern Baltic Sea when the direct effect of aerosol particles was
618 neglected. Despite the highly non-linear behavior of tropospheric O_3, the reduction in
619 the predicted O_3 concentrations indicates a high efficiency of aerosols to attenuate the

downward shortwave radiation, what is plausible once it was found that low PM_{10} concentrations have a capability to reduce ground level O_3 concentrations in a few ppb.

4. Summary and conclusions

The WRF-Chem community model has been used to evaluate the impact of vehicular emissions on the fine particles formation in the SPMA. Three thirty-one day simulations, covering a period from 7 August to 6 September 2012, have been performed. The aims were to evaluate the impact of fine particles formation (both inorganic and SOA) from gases emitted by road vehicles as well as the aerosol impacts on the ozone formation photochemistry. The results were compared with the measurements available from the NUANCE-SPS project.

The predicted temporal variations of meteorology, $PM_{2.5}$, PM_{10} and O_3 were found to agree well with the measurements at most of the sites during the entire simulation period. However, the predicted concentrations of $PM_{2.5}$, PM_{10} and O_3 (but in minor intensity) were lower than the observed values. This difference could be associated with an underestimation of the vehicular emissions and other emission sources such as industry, heating and cooking, which are not considered in this study. Wind speed and direction played an important role in the distribution of fine particles over the simulation domain. Backward trajectories analysis suggested that aerosol particles from biomass burning were transported to SPMA, impacting on the PM concentration over this region.

The baseline simulation (Case_0) showed that dust and sea salt aerosols made a contribution between 40 and 50% of the total PM_{10} concentration in the downtown SPMA. On the other hand, the Case_1, which represents simulations with gaseous emissions only, indicates that the emissions of primary gases coming mainly from

vehicles have a potential to form new particles between 20 and 30% in relation to the baseline $PM_{2.5}$ concentration found in the downtown SPMA. Finally, the Case_2, which represents simulations with aerosol-radiation feedback turned on, reveals a reduction in the surface O_3 concentration by around 2% in the afternoon (16:00 h; local time) when the aerosol-radiation feedback is taken into account.

This study provides a first step to understand the impact of vehicular emissions on the secondary particles formation in the SPMA. Nevertheless, more experimental campaigns are recommended for future work in order to characterize aerosols in ambient air and to improve their emission estimates so that a better understanding of physical and chemical properties and their formation can be established. This study also evaluates the importance of the VOCs in the formation of not only O_3 but also of fine particles. These compounds play an important role concerning health impacts and climate change, and the control of their concentrations requires the description of their formation mechanisms.

Appendix

The statistics used in this study are defined as follows:

1. Mean bias (MB)

$$MB = \frac{1}{n}\sum_{i=1}^{n}(M_i - O_i)$$

2. Mean fractional bias (MFB)

$$MFB = \frac{1}{n}\sum_{i=1}^{n}\frac{2(M_i - O_i)}{M_i + O_i}100\%$$

3. Mean fractional error (MFE)

$$MFE = \frac{1}{n}\sum_{i=1}^{n}\frac{2|M_i - O_i|}{M_i + O_i}100\%$$

[a10] **Comentário:** Two additional metrics (MFB and MFE) used for PM model evaluation were added.

4. Root mean square error UB ($RMSE_{UB}$)

$$RMSE_{UB} = \sqrt{\frac{1}{n}\sum_{i=1}^{n}[(M_i - \bar{M}) - (O_i - \bar{O})]^2}$$

5. Correlation coefficient (R)

$$r = \frac{\sum_{i=1}^{n}(M_i - \bar{M}) * (O_i - \bar{O})}{\sqrt{\sum_{i=1}^{n}(M_i - \bar{M})^2}\sqrt{\sum_{i=1}^{n}(O_i - \bar{O})^2}}$$

Where

$\bar{O} = \frac{1}{n}\sum_{i=1}^{n} O_i$ and $\bar{M} = \frac{1}{n}\sum_{i=1}^{n} M_i$ are the average values of the individual observed and predicted values, O_i and M_i, respectively. "n" is the number of observations.

5. Acknowledgments

Prashant Kumar, Angel Vara-Vela and Maria de Fatima Andrade thank the University of Surrey's International Relations Office for the Santander Postgraduate Mobility Award that helped Angel Vara to visit University of Surrey, UK, and develop this research article collaboratively. The authors from Universities of Surrey and Sao Paulo also acknowledge the collaborative funding received through the University Global Partnership Network (UGPN) to the project titled "*Emissions And Role Of Fine Aerosol Particles In Formation Of Clouds and Precipitation (eRAIN) - A demonstration study for the megacity, São Paulo*" for supporting this research work. Maria de Fatima

683 Andrade and Angel Vara-Vela acknowledged funding from the Coordination for the
684 Improvement of Higher Education Personnel (CAPES) and Research Foundation of the
685 State of Sao Paulo (FAPESP, project 2008/58104-8) that allowed the experimental
686 campaigns. The authors also thank the WRF-Chem developers, the NOAA's National
687 Geophysical Data Center, the NCAR's Data Support Section and Atmospheric
688 Chemistry Division, the Latin American Observatory (OLE2), the Sao Paulo
689 Environmental Protection Agency (CETESB), the OpenStreetMap Data Extracts, and
690 the NCAR Command Language (NCL) software for providing the tools and datasets
691 used in this research.

692

693 **6. References**

694 Ackermann, I. J., Hass, H., Memmesheimer, M., Ebel, A., Binkowski, F. S., and
695 Shankar, U.: Modal aerosol dynamics model for Europe: development and
696 first applications, Atmos. Environ., 32, 2981-2999, 1998.
697 Ahmadov, R., McKeen, S. A., Robinson, A. L., Bahreini, R., Middlebrook, A. M., de
698 Gouw, J. A., Meagher, J., Hsie, E. Y., Edgerton, E., Shaw, S., and Trainer,
699 M.: A volatility basis set model for summertime secondary organic
700 aerosols over the eastern United States in 2006, Journal of Geophysical
701 Research, 117, D06301, doi:10.1029/2011JD016831, 2012.
702 Albuquerque, T. T. A., Andrade, M. F., and Ynoue, R. Y.: Characterization of
703 atmospheric aerosols in the city of Sao Paulo, Brazil: comparisons between
704 polluted and unpolluted periods, Water Air Soil Pollution, 195, 201-213, 2011.
705 Anderson, L.: Ethanol fuel use in Brazil: air quality impacts, Energy Environ. Sci., 2,
706 1015-1037, 2009.

707 Andrade, M. F., Ynoue, R. Y., Freitas, E. D., Todesco, E., Vara-Vela, A., Ibarra, S.,
708 Martins, L. D., Martins, J. A., Carvalho, V. S. B.: Air quality forecasting system
709 for Southeastern Brazil, Front. Environ. Sci., 3, 1-14, 2015.
710 Andrade, M. F., Fornaro, A., Miranda, R. M., Kerr, A., Oyama, B., Andre, P. A., and
711 Saldiva, P.: Vehicle emissions and $PM_{2.5}$ mass concentrations in six
712 Brazilian cities, Air Quality, Atmosphere and Health, 5, 79-88, 2012.
713 Binkowski, F. S. and Shankar, U.: The regional particulate matter model, 1. Mode
714 description and preliminary results, Journal of Geophysical Research, 100,
715 26191-26209, 1995.
716 Birch, M. E. and Cary, R. A.: Elemental carbon-based method for occupational
717 monitoring of particulate diesel exhaust: methodology and exposure issues,
718 Aerosol Science and Technology, 25, 221-241, 1996.
719 Brito, J., Rizzo, L. V., Herckes, P., Vasconcellos, P. C., Caumo, S. E. S., Fornaro,
720 A., Ynoue, R. Y., Artaxo, P., and Andrade, M. F.: Physical-chemical
721 characterisation of the particulate matter inside two road tunnels in the Sao
722 Paulo Metropolitan Area, Atmos. Chem. Phys., 13, 12199-12213, 2013.
723 Brown, S. G., Lee, T., Roberts, P. T., and Collett, J. L. Jr.: Variations in the OM/OC
724 ratio of urban organic aerosol next to a major roadway, J. Air & Waste Manag. Assoc.,
725 63(12), 1422-1433, 2013.
726 Carvalho, V. S. B., Freitas, E. D., Martins, L. D., Martins, J. A., Mazzoli, C. R., and
727 Andrade, M. F.: Air quality status and trends over the Metropolitan Area of
728 Sao Paulo, Brazil as a result of emission control policies, Environmental
729 Science & Policy, 47, 68-79, 2015.
730 Castanho, A. D. A. and Artaxo, P.: Sao Paulo aerosol source apportionment for
731 wintertime and summertime, Atmos. Environ., 35, 4889-4902, 2001.

732 Costa, R. C. and Sodré, J. R.: Hydrous ethanol vs. gasoline-ethanol blend: Engine
733 performance and emissions, Fuel, 89, 287-293, 2010.
734 CETESB-Companhia de Tecnologia de Saneamento Ambiental. Relatorio Anual
735 de Qualidade do Ar no Estado de Sao Paulo 2012, Sao Paulo, 2013.
736 CETESB-Companhia de Tecnologia de Saneamento Ambiental. Emissões
737 veiculares no Estado de São Paulo 2011, Sao Paulo, 2012.
738 CETESB-Companhia de Tecnologia de Saneamento Ambiental. Relatorio Anual
739 de Qualidade do Ar no Estado de Sao Paulo 2009, Sao Paulo, 2010.
740 Chang, J. S., Binkowki, F. S., Seaman, N. L., McHenry, J. N., Samson, P. J.,
741 Stockwell, W. R., Walcek, C. J., Madronich, S., Middleton, P. B., Pleim, J. E.,
742 and Lansford, H. H.: The regional acid deposition model and engineering
743 model, State-of-Science/Technology, Report 4, National Acid Precipitation
744 Assessment Program, Washington, DC, 1989.
745 Draxler, R. R. and Hess, G. D.: An overview of the HYSPLIT 4 modelling system of
746 trajectories, dispersion, and deposition, Aust. Meteor. Mag., 47, 295-308, 1998.
747 Emmons, L. K., Walters, S., Hess, P. G., Lamarque, F., Pfister, G. G., Fillmore, D.,
748 Granier, C., Guenther, A., Kinnison, D., Laepple, T., Orlando, J., Tie, X.,
749 Tyndall, G., Wiedinmyer, C., Baughcum, S. L., and Kloster, S.: Description
750 and evaluation of the Model for Ozone and Related chemical Tracers, version
751 4 (MOZART-4), Geosci. Model Dev., 3, 43-67, 2010.
752 Ginoux, P., Chin, M., Tegen, I., Prospero, J. M., Holben, B., Dubovik, O., and Lin,
753 S-J.: Sources and distributions of dust aerosols simulated with the GOCART
754 model, Journal of Geophysical Research, 106, 20,255-20,273, 2001.

755 Gong, S. L.: A parameterization of sea-salt aerosol source function for sub- and super-
756 micron particles, Global Biogeochemical Cycles, 17, 1097,
757 doi:10.1029/2003GB002079, 2003.
758 Gorin, C. A., Collett, J. L. Jr., and Herckes, P.: Wood smoke contribution to winter
759 aerosol in Fresno, CA, J. Air & Waste Manag. Assoc., 56(11), 1584-1590,
760 2006.
761 GrEC-Grupo de Estudos Climáticos. Relatório climatológico mensal, previsão climática
762 para o Brasil: Set-Out-Nov/2012, Sao Paulo, 2012a. Available at:
763 www.grec.iag.usp.br/link_grec_old/relatorios_climatologicos/2012/agosto/.
764 GrEC-Grupo de Estudos Climáticos. Relatório climatológico mensal, monitoramento
765 climático para o Brasil: Set/2012, Sao Paulo, 2012b. Available at:
766 www.grec.iag.usp.br/link_grec_old/relatorios_climatologicos/2012/setembro/.
767 Grell, G. A., Peckham, S. E., Schmitz, R., McKeen, S. A., Wilczak, J., and Eder, B.:
768 Fully coupled "online" chemistry within the WRF model, Atmos. Environ., 39,
769 6957-6975, 2005.
770 Guenther, A. B., Zimmerman, P. R., Harley, P. C., Monson, R. K., and Fall, R.:
771 Isoprene and monoterpene emission rate variability: model evaluations and
772 sensitivity analyses, Journal of Geophysical Research, 98D, 12609-12617,
773 1993.
774 Guenther, A., Zimmerman, P., and Wildermuth, M.: Natural volatile organic
775 compound emission rateestimates for US woodland landscapes, Atmos.
776 Environ., 28, 1197-1210, 1994.
777 Fast, J. D., Gustafson, W. I., Easter, R. C., Zaveri, R. A., Barnard, J. C., Chapman,
778 E. G., Grell, G. A., and Peckham, S. E.: Evolution of ozone, particulates, and
779 aerosol direct radiative forcing in the vecinity of Houston using a fully

780 coupled meteorology-chemistry-aerosol module, Journal of Geophysical
781 Research, 111, D21305, doi:10.1029/2005JD006721, 2006.
782 Forkel, R., Werhahn, J., Hansen, A. B., McKeen, S., Peckham, S., Grell, G., and
783 Suppan, P.: Effect of aerosol-radiation feedback on regional air quality - A
784 case study with WRF/Chem, Atmospheric Environment, 53, 202-211, 2012.
785 Heal, M. R., Kumar, P., and Harrison, R. M.: Particles, air quality, policy and health,
786 Chem. Soc. Rev., 41, 6606-6630, 2012.
787 Jenkin, M. E. and Clemitshaw, K. C.: Ozone and other secondary photochemical
788 pollutants: chemical processes governing their formation in the planetary
789 boundary layer, Atmos. Environ., 34, 2499-2527, 2000.
790 Kroll, J. H. and Seinfeld, J. H.: Chemistry of secondary organic aerosol: Formation and
791 evolution of low-volatility organics in the atmosphere, Atmos. Environ., 42,
792 3593-3624, 2008.
793 Kulmala, M., Laaksonen, A., and Pirjola, L.: Parameterization for sulphuric
794 acid/water nucleation rates, Journal of Geophysical Research, 103, 8301-
795 8307, 1998.
796 Kumar, P., Morawska, L., Birmili, W., Paasonen, P., Hu, M., Kulmala, M., Harrison,
797 R.M., Norford, L., and Britter, R.: Ultrafine particles in cities, Environment
798 International, 66, 1-10, 2014.
799 Kumar, P., Robins, A., Vardoulakis, S., and Britter, R.: A review of the characteristics
800 of nanoparticles in the urban atmosphere and the prospects for developing
801 regulatory control, Atmos. Environ., 44, 5035-5052, 2010.
802 Kumar, P., Ketzel, M., Vardoulakis, S., Pirjola, L., Britter, R.: Dynamics and dispersion
803 modelling of nanoparticles from road traffic in the urban atmospheric
804 environment - a review, J. Aerosol Sci., 42, 580-603, 2011.

Li, G., Bei, N., Tie, X., and Molina, L. T.: Aerosol effects on the photochemistry in Mexico City during MCMA-2006/MILAGRO campaign, Atmos. Chem. Phys., 11, 5169-5182, 2011a.

Li, G., Zavala, M., Lei, W., Tsimpidi, A. P., Karydis, V. A., Pandis, S. N., Canagaratna, M. R., and Molina, L. T.: Simulations of organic aerosol concentrations in Mexico City using the WRF-Chem model during the MCMA-2006/MILAGRO campaign, Atmos. Chem. Phys., 11, 3789-3809, 2011b.

Li, G., Zhang, R., and Fan, J.: Impacts of black carbon aerosol on photolysis and ozone, Journal of Geophysical Research, 110, D23206, doi:10.1029/2005JD005898, 2005.

Marple, V. A., Rubow, K. L., Ananth, G. P., and Fissan, H. J.: Micro-Orifice Uniform Deposit Impactor, Journal of Aerosol Science, 17, 489-494, 1986.

Martins, L. D., Vasconcellos, P. C., Carvalho, L. F., Andrade, M. F.: Estimated impact of biogenic hydrocarbon emissions on photochemical oxidant formation in Sao Paulo during two periods of the winters of 1999-2000, Revista Brasileira de Meteorologia, 21, 190-200, 2006.

McMurry, P., Shepherd, M., and Vickery, J.: Particulate Matter Science for Policy Makers: A NARSTO Assessment, Cambridge University Press, Cambridge, England, 2004.

Middleton, P., Stockwell, W. R., and Carter, W. P. L.: Aggregation and analysis of volatile organic compound emissions for regional modelling, Atmos. Environ., 24A, 1107-1133, 1990.

828 Miranda, R. M. and Andrade, M. F.: Physicochemical characteristics of atmospheric
829 aerosols during winter in the Sao Paulo Metropolitan Area in Brazil, Atmos.
830 Environ., 39, 6188-6193, 2005.
831 Monahan, E. C., Spiel, D. E., Davidson, K. L.: A model of marine aerosol generation
832 via whitecaps and wave disruption. In: Monahan, E. C., MacNiocaill, G. D.
833 (Eds.), Oceanic Whitecaps. Reidel Publishing Company, Norwell, Mass, 167-
834 174, 1986.
835 Muñoz, A. G., López, P., Velásquez, R., Monterrey, L., León, G., Ruiz, F., Recalde,
836 C., Cadena, J., Mejía, R., Paredes, M., Bazo, J., Reyes, C., Carrasco, G.,
837 Castellón, Y., Villarroel, C., Quintana, J., and Urdaneta, A.: An
838 Environmental Watch System for the Andean Countries: El Observatorio
839 Andino, Bull. Amer. Meteor. Soc., 91, 1645-1652, 2010.
840 Muñoz, A. G., Ruiz-Carrascal, D., Ramírez, P., León, G., Quintana, J., Bonilla, A.,
841 Torres, W., Pastén, M., and Sánchez, O.: Risk Management at the Latin
842 American Observatory, in: Risk Management–Current Issues and Challenges,
843 InTech Publications, doi:10.5772/50788, 533-556, 2012.
844 Nogueira, T., Dominutti, P. A., De Carvalho, L. R. F., Fornaro, A., and Andrade, M.
845 F.: Formaldehyde and acetaldehyde measurements in urban atmosphere
846 impacted by the use of ethanol biofuel: Metropolitan Area of Sao Paulo, 2012-
847 2013, Fuel, 134, 505-513, 2014.
848 Odum, J. R., Hoffmann, T., Bowman, F., Collins, D., Flagan, R. C., and Seinfeld, J.
849 H.: Gas/particle partitioning and secondary organic aerosol yields,
850 Environmental Science Technology, 30, 2580-2585, 1996.
851 Pankow, J. F.: An absorption model of the gas aerosol partitioning involved in the
852 formation of secondary organic aerosol, Atmos. Environ., 28, 185-188, 1994a.

853 Pankow, J. F.: An absorption model of the gas aerosol partitioning involved in the
854 formation of secondary organic aerosol, Atmos. Environ., 28, 189-93, 1994b.
855 Pérez-Martínez, P. J., Andrade, M. F., and Miranda, R. M.: Traffic-related air quality
856 trends in Sao Paulo, Brazil, J. Geophys. Res. Atmos., 120, 6290-6304,
857 doi:10.1002/2014JD022812, 2015.
858 Pérez-Martínez, P. J., Miranda, R. M., Nogueira, T., Guardani, M. L., Fornaro, A.,
859 Ynoue, R., and Andrade, M. F.: Emission factors of air pollutants from
860 vehicles measured inside road tunnels in Sao Paulo: case study comparison,
861 Int. J. Environ. Sci. Technol., 11, 2155-2168, 2014.
862 Real, E. and Sartelet, K.: Modelling of photolysis rates over Europe: impact on
863 chemical gaseous species and aerosols, Atmos. Chem. Phys., 11, 1711-1727,
864 2011.
865 Salvo, A. and Geiger, F. M.: Reduction in local ozone levels in urban Sao Paulo due to
866 a shift from ethanol to gasoline use, Nature Geoscience, 7, 450-458,
867 doi:10.1038/ngeo2144, 2014.
868 Saxena, P., Hudischewskyj, A. B., Seigneur, C., and Seinfeld, J. H.: A comparative
869 study of equilibrium approaches to the chemical characterization of
870 secondary aerosols, Atmos. Environ., 20, 1471-1483, 1986.
871 Schell, B., Ackerman, I. J., Hass, H., Binkowski, F. S., and Ebel, A.: Modelling the
872 formation of secondary organic aerosol within a comprehensive air quality
873 model system, Journal of Geophysical Research, 106, 28275-28293, 2001.
874 Seinfeld, J. H. and Pandis, S. N.: Atmospheric Chemistry and Physics: from air
875 pollution to climate change, Second Edition, Jhon Wiley, New Jersey,
876 2006.

877 Shrivastava, M., Berg, L. K., Fast, J. F., Easter, R. C., Laskin, A., Chapman, E. G.,
878 Gustafson Jr, W. I., Liu, Y., and Berkowitz, C. M.: Modelling aerosols and
879 their interactions with shallow cumuli during the 2007 CHAPS field study,
880 Journal of Geophysical Research: Atmospheres, 118, 1343-1360, 2013.
881 Taylor, K. E.: Summarizing multiple aspects of model performance in a single diagram,
882 Journal of Geophysical Research, 106(D7), 7183-7192,
883 doi:10.1029/2000JD900719, 2001.
884 Tuccella, P., Curci, G., Visconti, G., Bessagnet, B., Menut, L., and Park, R. J.:
885 Modelling of gas and aerosol with WRF-Chem over Europe: Evaluation and
886 sensitivity study, Journal of Geophysical Research, 117, D03303,
887 doi:10.1029/2011JD016302, 2012.
888 Vasconcellos, P. C., Souza, D. Z., Sanchez-Ccoyllo, O. R., Bustillos, J. O. V., Lee,
889 H., Santos, F. C., Nascimento, K. H., Araujo, M. P., Saarnio, K., Teinila, K.,
890 and Hillamo, R.: Determination of anthropogenic and biogenic
891 compounds on atmospheric aerosol collected in urban, biomass burning
892 and forest areas in Sao Paulo, Brazil, Science of the Total Environment, 408,
893 5836-5844, 2010.
894 Vieira-Filho, M. S., Pedrotti, J. J., and Fornaro, A.: Contribution of long and mid-range
895 transport on the sodium and potassium concentrations in rainwater samples, Sao
896 Paulo megacity, Brazil, Atmos. Environ., 79, 299-307, 2013.
897 Wedding, J. B., Weigand, M., John, W., and Wall, S.: Sampling effectiveness of the
898 inlet to the dichotomous sampler, Environ. Sci. Technol., 14(11), 1367-1370,
899 1980.

900 Ynoue, R. Y. and Andrade, M. F.: Size-resolved mass balance of aerosol particles over
901 the Sao Paulo Metropolitan Area of Brazil, Aerosol Science and Technology, 1,
902 52-62, 2004.

903 Table 1. Description of aerosol sampling campaigns performed at IAG-USP.

Parameter	Sampling frequency	Period of sampling	Sampling device
Aerosol mass size distribution	24 hours	July-September	MOUDI impactor
$PM_{2.5}$ and PM_{10} concentration	12 hours	July-September	Dichotomous sampler
OC and EC concentration	12 hours	August-September	Sunset OC-EC analyser

904
905

906 Table 2. Description of measurement sites.

Site	Initials	Latitude	Longitude	Classification	Measured species
Nossa S. do	NSO	-23.4796	-46.6916	Urban	PM_{10}, O_3
Santana	SAN	-23.5055	-46.6285	Urban	PM_{10}
Parque D.	PDP	-23.5448	-46.6276	Urban	PM_{10}, O_3
Mooca	MOO	-23.5497	-46.5984	Urban	PM_{10}, O_3
Cerqueira	CCE	-23.5531	-46.6723	Urban	PM_{10}
IAG-USP	IAG-USP	-23.5590	-46.7330	Suburban	PM_{10}, $PM_{2.5}$, OC, EC, aerosol mass size distrib.[a]
IPEN-USP	IPEN-USP	-23.5662	-46.7374	Suburban	$PM_{2.5}$, O_3, NOx, CO
Ibirapuera	IBI	-23.5914	-46.6602	Suburban	PM_{10}, O_3, NOx, CO
Congonhas	CON	-23.6159	-46.6630	Urban	PM_{10}, $PM_{2.5}$
AF-IAG	AF-IAG	-23.6500	-46.6167	Suburban	T, RH, WS, WD[b]
Santo	SAM	-23.6545	-46.7095	Urban	PM_{10}
Interlagos	INT	-23.6805	-46.6750	Urban	PM_{10}, O_3, T, RH, WS,

907 [a]includes SO_4^{2-}, NO_3^-, NH_4^+, Na^+, Cl^- and PM_{10}.

908 [b]T, RH, WS, and WD denote temperature, relative humidity, wind speed and wind

909 direction, respectively.

910

[a11] Comentário: Added.

911 Table 3. Selected WRF-Chem configuration options.

Atmospheric Process	WRF-Chem option
Longwave radiation	RRTM
Shortwave radiation	Goddard
Surface layer	Monin-Obukhov
Land surface	Noah
Boundary layer	YSU
Cumulus clouds[a]	Grell 3D
Cloud microphysics	Lin
Gas-phase chemistry	RADM2
Aerosol chemistry	MADE/SORGAM
Photolysis	Fast-J

912 [a]Outer domains only

913

914 Table 4. Description of WRF-Chem simulations.

Label	Description
Case_0	Emission of gases
(Baseline simulation)	Emission of aerosols
	Aerosol-radiation feedback turned on
Case_1	Emission of gases
	No emission of aerosols
	Aerosol-radiation feedback turned on
Case_2	Emission of gases
	Emission of aerosols
	Aerosol-radiation feedback turned off

915

916

Table 5. Performance statistics for WRF-Chem predictions at all sites[a]

Index	$PM_{2.5}$	PM_{10}	O_3	NOx	CO	T	RH	WS	WD
MB	-8.84	-14.10	-0.85	-8.75	-0.27	0.65	-5.74	0.54	31.12
MFB (%)	-47.62	-38.19	22.63	12.68	-32.53	1.94	-7.95	41.21	31.66
MFE (%)	47.90	39.90	72.85	82.82	80.93	14.16	23.84	71.12	54.40
$RMSE_{UB}$	6.83	10.59	27.45	30.35	0.57	3.21	20.06	1.08	79.38
R	0.73	0.72	0.63	0.42	0.54	0.71	0.62	0.41	0.43

[a]Values are averaged from all the individual indexes found at the measurement sites. Individual indexes are calculated from both hourly observed and predicted values.

[a12] Comentário: The analysis of winds was reformulated considering wind speed and direction instead of zonal and meridional wind components.

Figure 1. Downtown area of the 3 km modelling domain (d03) showing the locations of measurement sites and WRF topography in the vicinity of the SPMA. Red dots represent sites with information on O_3 and PM. Yellow dots represent only sites with information on PM. Blue dot represents the location of the IAG-USP's climatological station.

Figure 2. Emission rates for Aromatic VOCs at 19 UTC in the 3 km modelling domain.

Figure 3. Hourly accumulated precipitation and relative humidity observed at the IAG-USP's climatological station during the study period.

Figure 4. HYSPLIT three-day backward trajectories and locations of fires in Sao Paulo State and part of central-west region of Brazil. Pink markers represent the observed fire locations during the study period considering different satellite products (GOES, AQUA, TERRA, NOAA). The backward trajectories starting at IAG-USP were calculated for the days 9 and 31 August and 5 September 2012 at three different altitudes: 500 m (red lines), 1000 m (blue lines), and 2000 m (green lines).

Figure 5. Daily (top), diurnal (bottom), and nocturnal (middle) mean concentrations for EC, OC, PM_{10}, $PM_{2.5-10}$, $PM_{2.5}$ (left panels), and Na, Fe_2SO_3, SiO_2, K_2O, and S (right panels). The $PM_{2.5-10}$ aerosol variable is defined as particulate matter with aerodynamic diameter between 2.5 and 10 μm. The grey line indicates the WHO air quality standard for PM2.5 (25 μg m^{-3}).

Figure 6. The predicted average of wind vectors at 10 m and temperature at 2 m from the baseline simulation (Case_0) for the whole study period in the 3 km modelling domain. Blue dots represent the locations of the measurement sites,

whereas cyan numbers represent the observed average temperature in those sites: 17.7 °C in AF-IAG and 17.8 °C in INT.

Figure 7. The observed and predicted daily variations of $PM_{2.5}$ concentrations at three sites in SPMA for the 3 km modelling domain.

Figure 8. The observed and predicted daily variations of PM_{10} concentrations at ten sites in SPMA for the 3 km modelling domain.

Figure 9. The observed and predicted hourly variations of O_3 concentrations at six sites in SPMA for the 3 km modelling domain.

Figure 10. Taylor diagram (Taylor, 2001) showing the individual correlation coefficients, mean biases, and normalized standard deviations for the PM_{10}, $PM_{2.5}$, OC and EC concentrations.

[a13] Comentário: Modified.

Figure 11. The predicted average surface distribution of $PM_{2.5}$ concentrations for the whole study period in the 3 km modelling domain. Red dots represent the locations of the measurement sites with information on $PM_{2.5}$, whereas cyan numbers represent the observed average $PM_{2.5}$ concentration in those sites: 23.4 µg m^{-3} in IPEN-USP, 21.3 µg m^{-3} in IAG-USP, and 22.2 µg m^{-3} in CON.

Figure 12. The predicted average surface distribution of PM_{10} concentrations for the whole study period in the 3 km modelling domain. Red dots represent the locations of the measurement sites with information on PM_{10}, whereas cyan numbers represent the observed average PM_{10} concentration in those sites: 49.5 µg m^{-3} in IAG-USP and 38.7 µg m^{-3} in CON.

Figure 13. The predicted average surface distribution of the $PM_{2.5}$:PM_{10} ratio for the whole study period in the 3 km modelling domain. Red dots represent the locations of the measurement sites with information on both $PM_{2.5}$ and PM_{10},

whereas cyan numbers represent the observed average $PM_{2.5}$:PM_{10} ratio in those sites: 0.43 in IAG-USP and 0.57 in CON.

Figure 14. The observed and predicted daily variations of OC and EC concentrations at IAG-USP.

Figure 15. The observed and predicted average aerosol mass size distribution for SO_4, NO_3, NH_4, Na, Cl, and other PM_{10} constituents at IAG-USP. The observed aerosol distributions were collected in ten size classes using a rotated impactor (MOUDI) and joined adequately according to the three modes used by the MADE aerosol scheme: Aitken (<0.1 μm), accumulation (0.1-1 μm) and coarse (>1 μm). The five inorganic ions carried in MADE are only calculated for the Aitken and accumulation modes. The WRF's PM_{10} aerosol variable does not include neither OC nor EC for this comparison.

Figure 16. The observed and predicted average contributions for the main identified constituents of $PM_{2.5}$ at IAG-USP.

Figure 17. The impact of (a) emissions of primary gases on the fine particles formation, (b) emissions of dust-sea salt aerosols on the PM_{10} concentration, and (c) aerosol direct effect on the ground level O_3 concentrations at 16:00 h (local time).

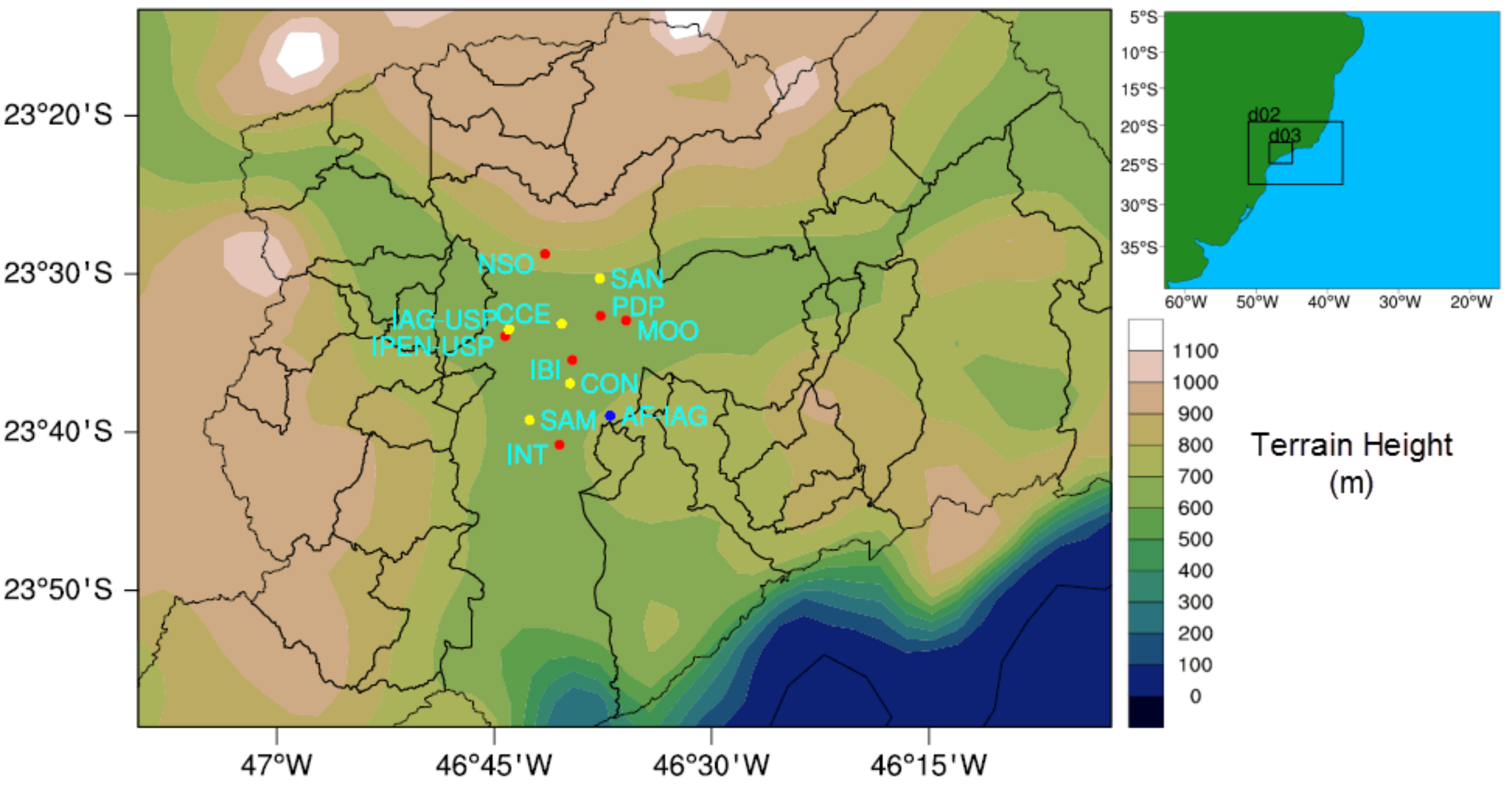
23°20'S
23°30'S
23°40'S
23°50'S
47°W
46°45'W
46°30'W
46°15'W
NSO
SAN
PDP
MOO
IAG-USP
CCE
IPEN-USP
IBI
CON
SAM
AF-IAG
INT
5°S
10°S
15°S
20°S
25°S
30°S
35°S
60°W
50°W
40°W
30°W
20°W
d02
d03
1100
1000
900
800
700
600
500
400
300
200
100
0
Terrain Height
(m)

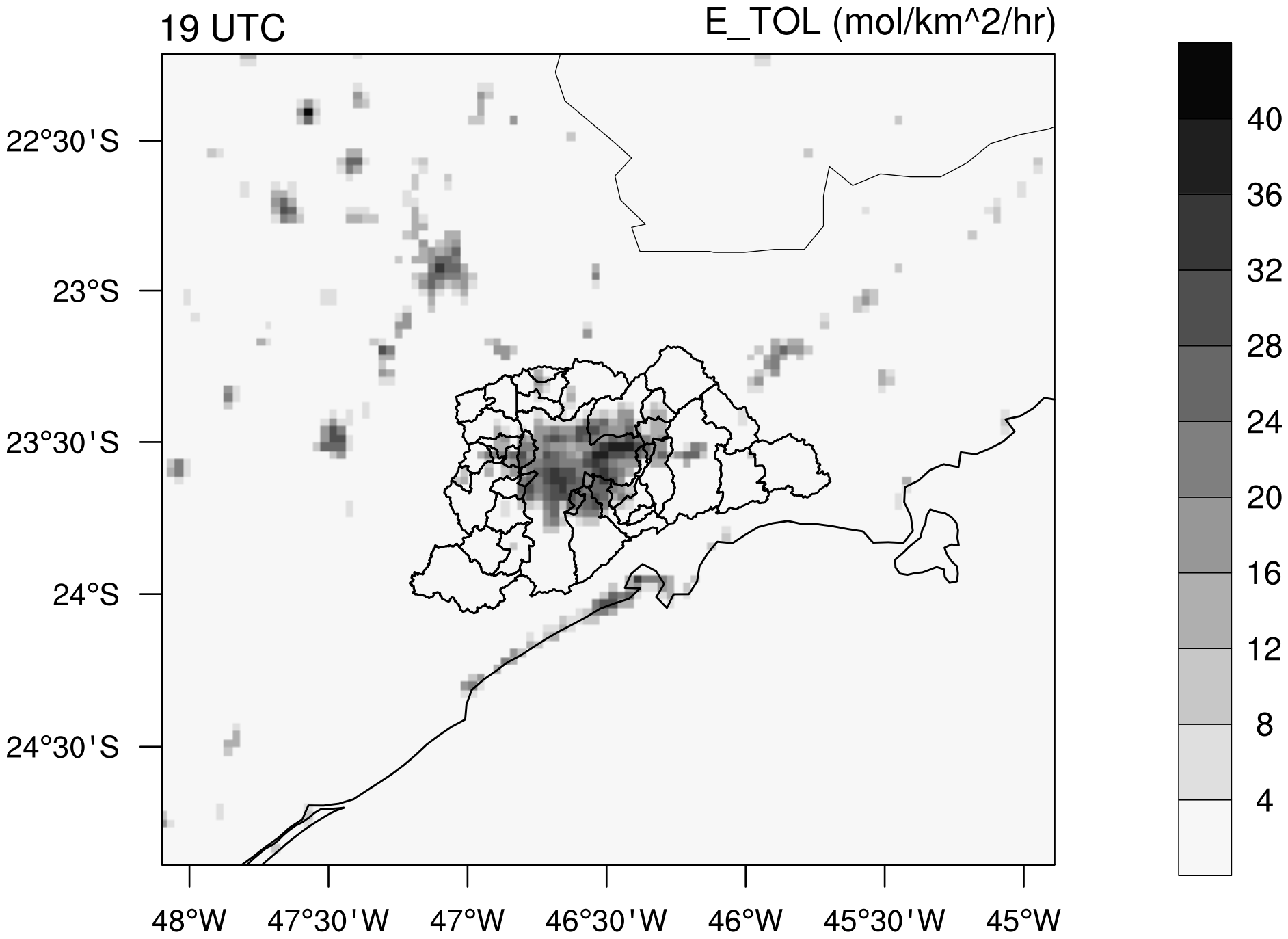
19 UTC
E_TOL (mol/km^2/hr)
22°30'S
23°S
23°30'S
24°S
24°30'S
48°W
47°30'W
47°W
46°30'W
46°W
45°30'W
45°W
40
36
32
28
24
20
16
12
8
4

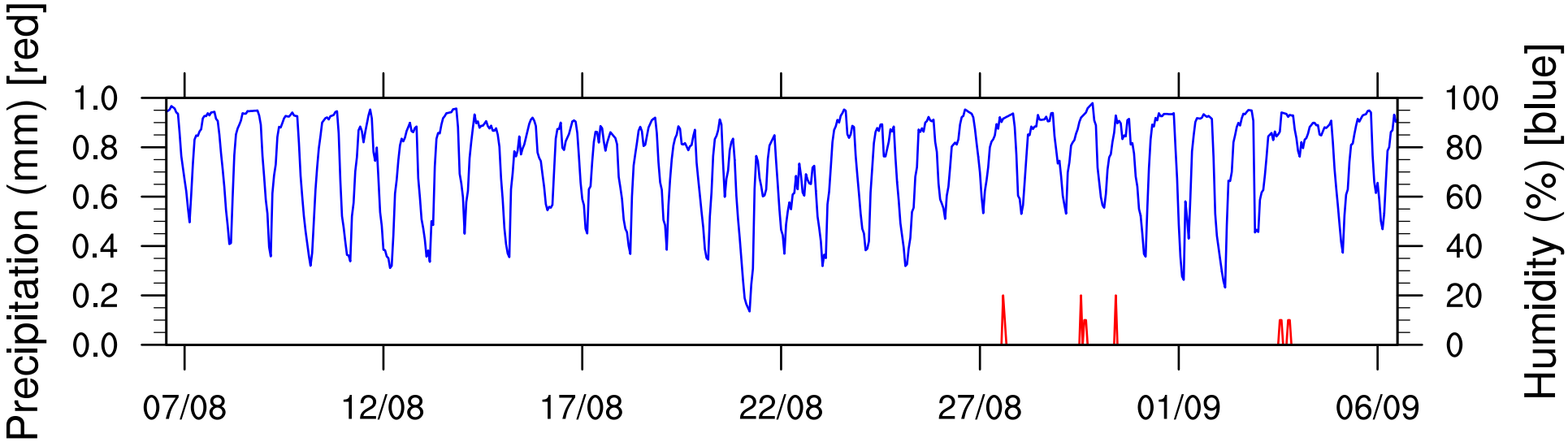
Precipitation (mm) [red]
1.0
0.8
0.6
0.4
0.2
0.0
100
80
60
40
20
0
Humidity (%) [blue]
07/08
12/08
17/08
22/08
27/08
01/09
06/09

8/9/2012 3 tarde/noite

HYSPLIT

Minas Gerais

Espírito Santo

Mato Grosso do Sul

09/02/2012 18 UTC - 500 m

09/02/2012 18 UTC - 2000 m

Rio de Janeiro

09/02/2012 18 UTC - 1000 m

08/06/2012 18 UTC - 500 m

08/06/2012 18 UTC - 2000 m

Paraguai

Assunção

Paraná

Itapúa

Chaco

Santa Catarina

Iberá Wetlands

Rio Grande do Sul

Lagoa dos Patos

Rivera

Uruguai

Lagoa Mirim

08/28/2012 18 UTC - 500 m

08/28/2012 18 UTC - 1000 m

Monitoramento de Queimadas

Legendas
- Goes
- Aqua
- Terra
- MModis-01D
- NOAA-12
- NOAA-12D
- NOAA-14
- NOAA-15
- NOAA-15D
- NOAA-17
- NOAA-18
- NOAA-18D
- Meteosat

Image Landsat
© 2015 Google
Data SIO, NOAA, U.S. Navy, NGA, GEBCO
US Dept of State Geographer

Google earth

Data das imagens: 4/9/2013 lat -25.364396° lon -46.185469° elev -108 m altitude do ponto de visão 2297.00 km

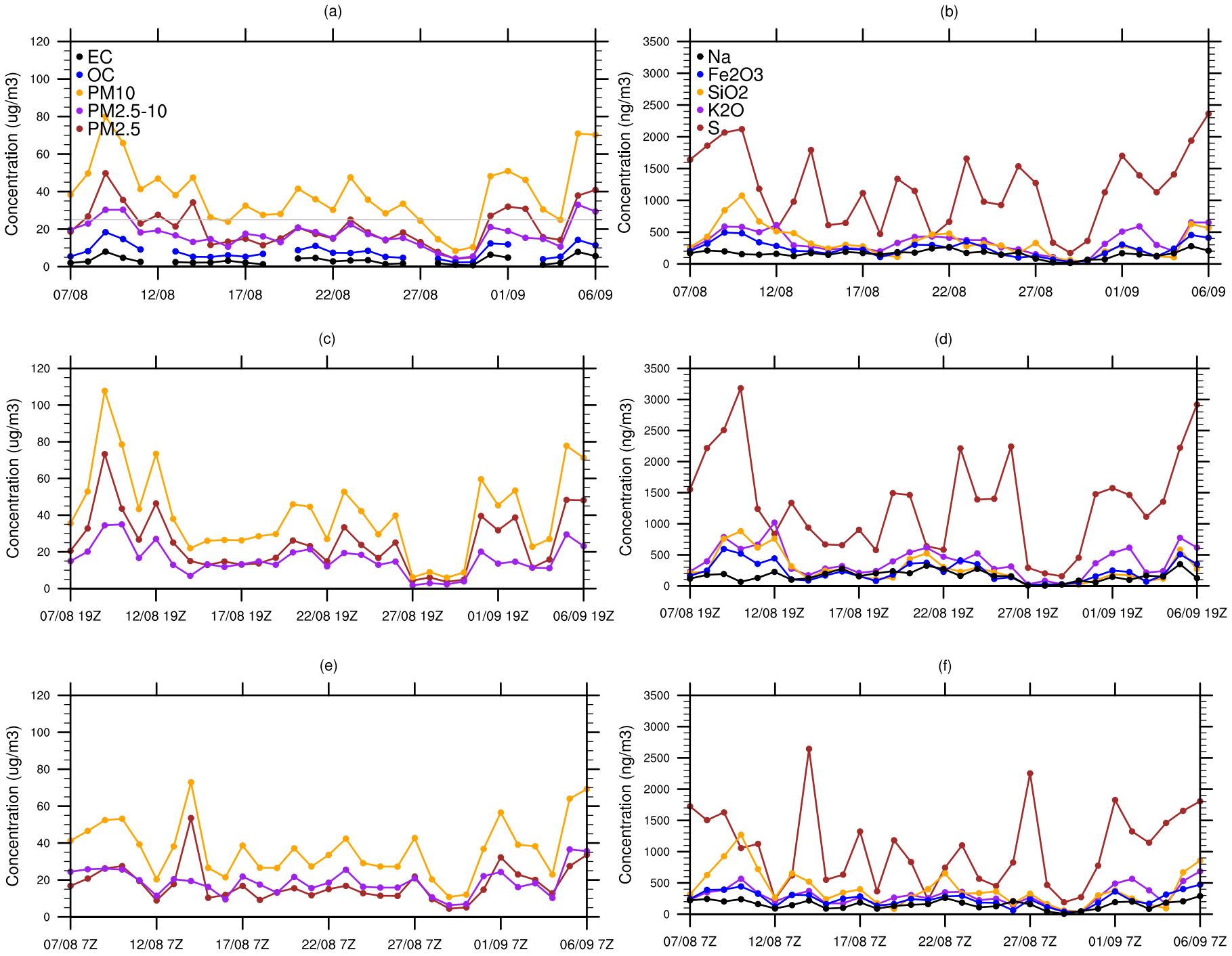
(a)
Concentration (ug/m3)
EC
OC
PM10
PM2.5-10
PM2.5
07/08
12/08
17/08
22/08
27/08
01/09
06/09
(b)
Concentration (ng/m3)
Na
Fe2O3
SiO2
K2O
S
(c)
Concentration (ug/m3)
07/08 19Z
12/08 19Z
17/08 19Z
22/08 19Z
27/08 19Z
01/09 19Z
06/09 19Z
(d)
Concentration (ng/m3)
(e)
Concentration (ug/m3)
07/08 7Z
12/08 7Z
17/08 7Z
22/08 7Z
27/08 7Z
01/09 7Z
06/09 7Z
(f)
Concentration (ng/m3)

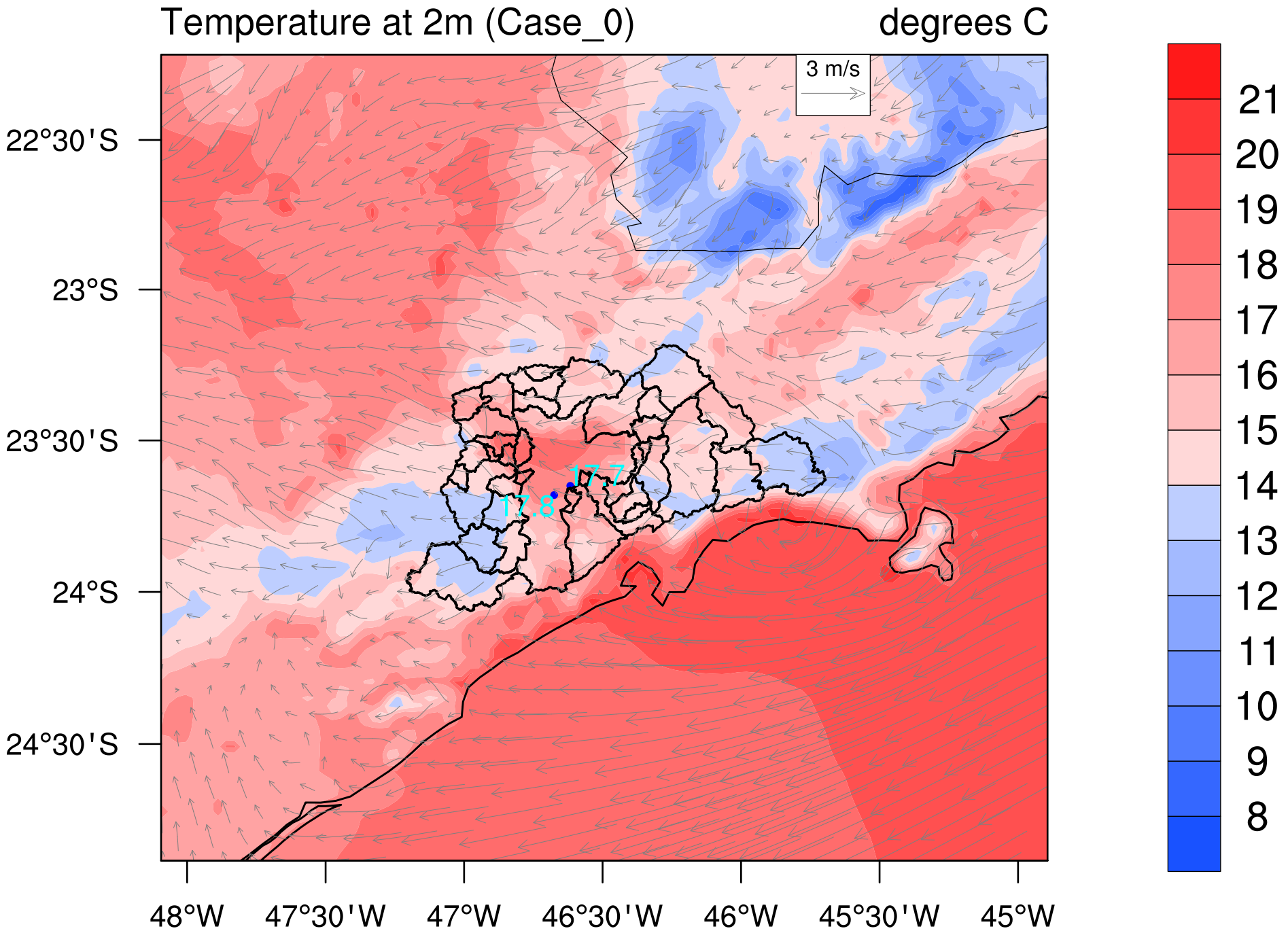
Temperature at 2m (Case_0)
degrees C
3 m/s
22°30'S
23°S
23°30'S
24°S
24°30'S
48°W
47°30'W
47°W
46°30'W
46°W
45°30'W
45°W
17.7
17.8
21
20
19
18
17
16
15
14
13
12
11
10
9
8

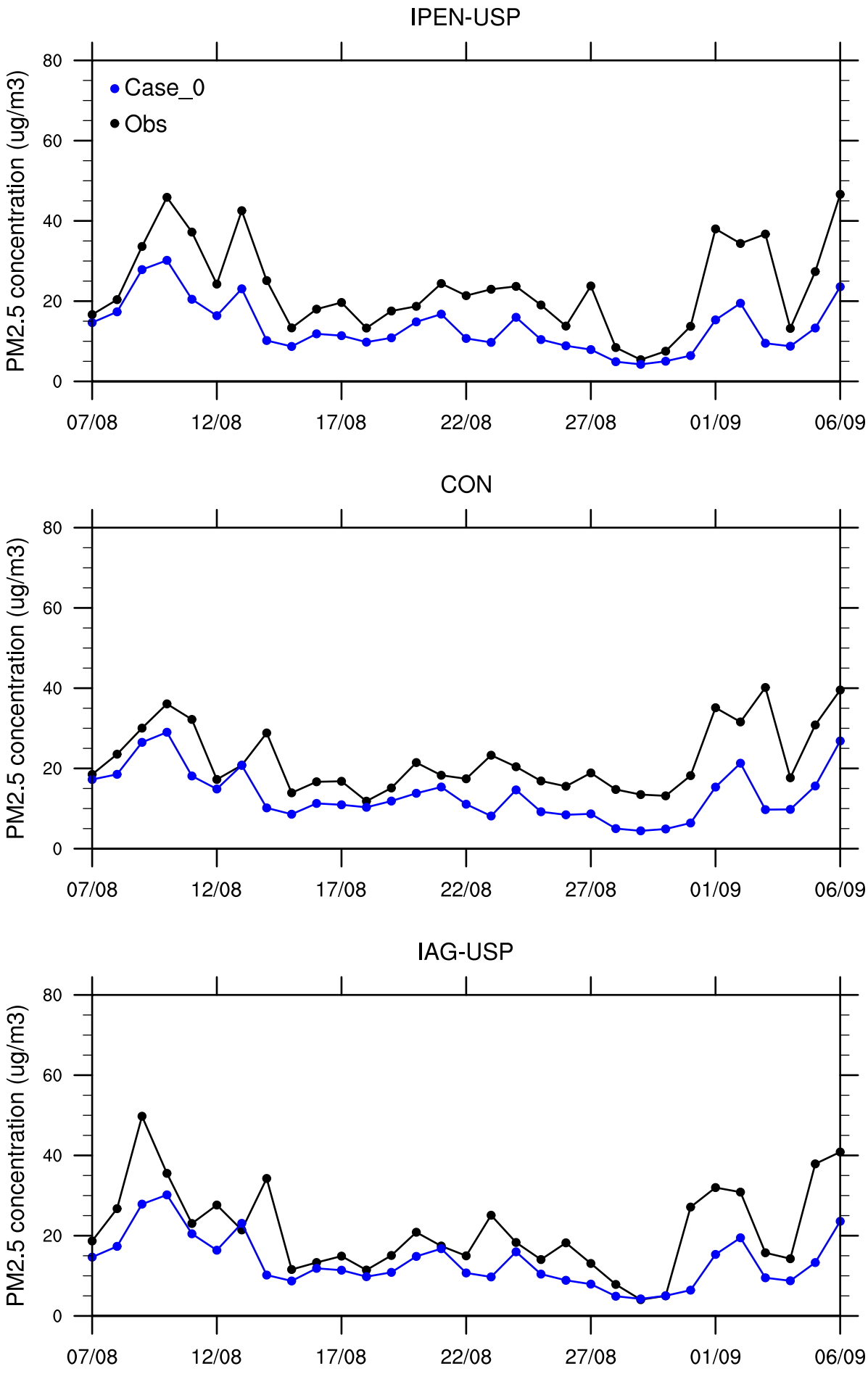
IPEN-USP
Case_0
Obs
PM2.5 concentration (ug/m3)
0
20
40
60
80
07/08
12/08
17/08
22/08
27/08
01/09
06/09
CON
PM2.5 concentration (ug/m3)
0
20
40
60
80
07/08
12/08
17/08
22/08
27/08
01/09
06/09
IAG-USP
PM2.5 concentration (ug/m3)
0
20
40
60
80
07/08
12/08
17/08
22/08
27/08
01/09
06/09

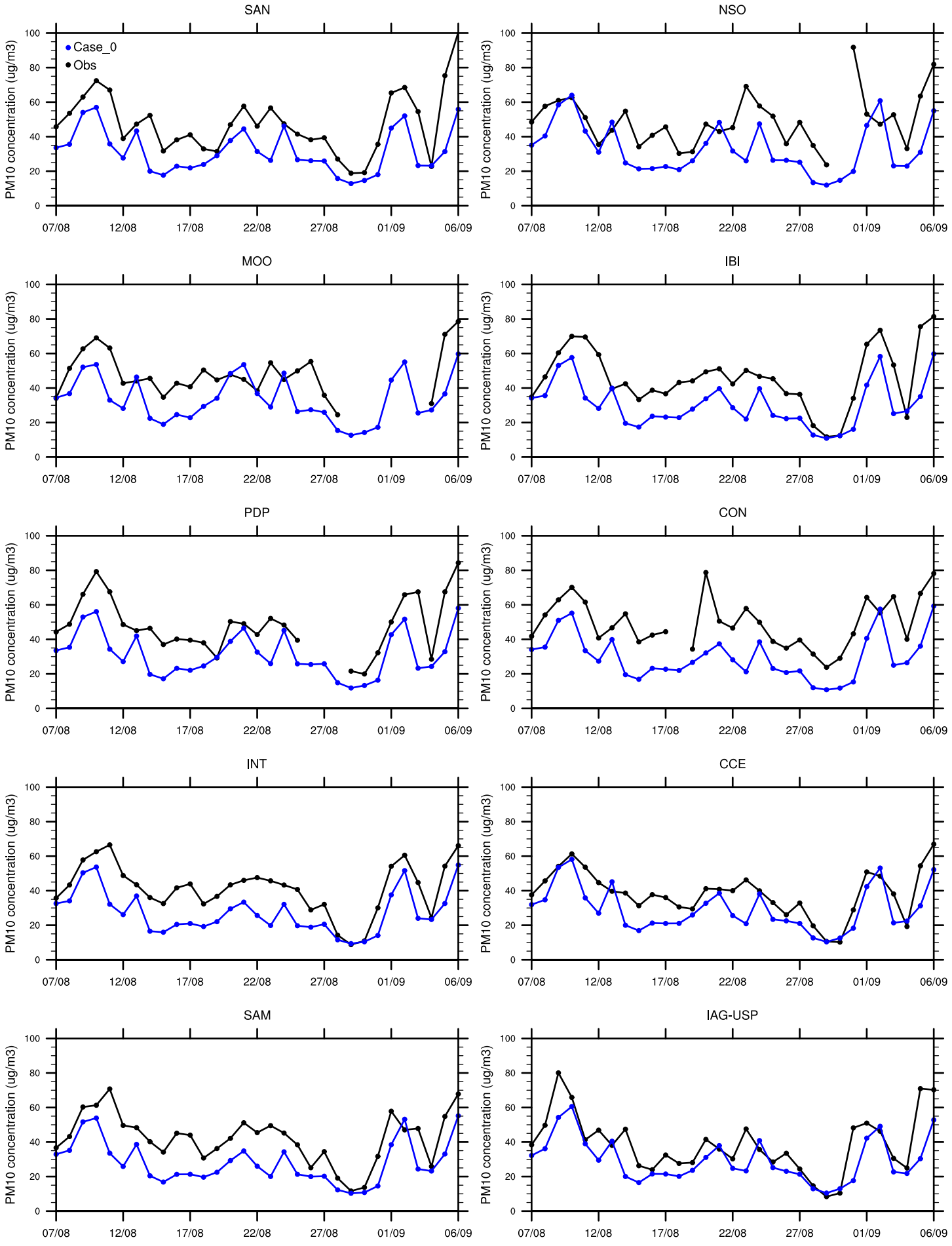
SAN
NSO
MOO
IBI
PDP
CON
INT
CCE
SAM
IAG-USP
Case_0
Obs
PM10 concentration (ug/m3)
0
20
40
60
80
100
07/08
12/08
17/08
22/08
27/08
01/09
06/09

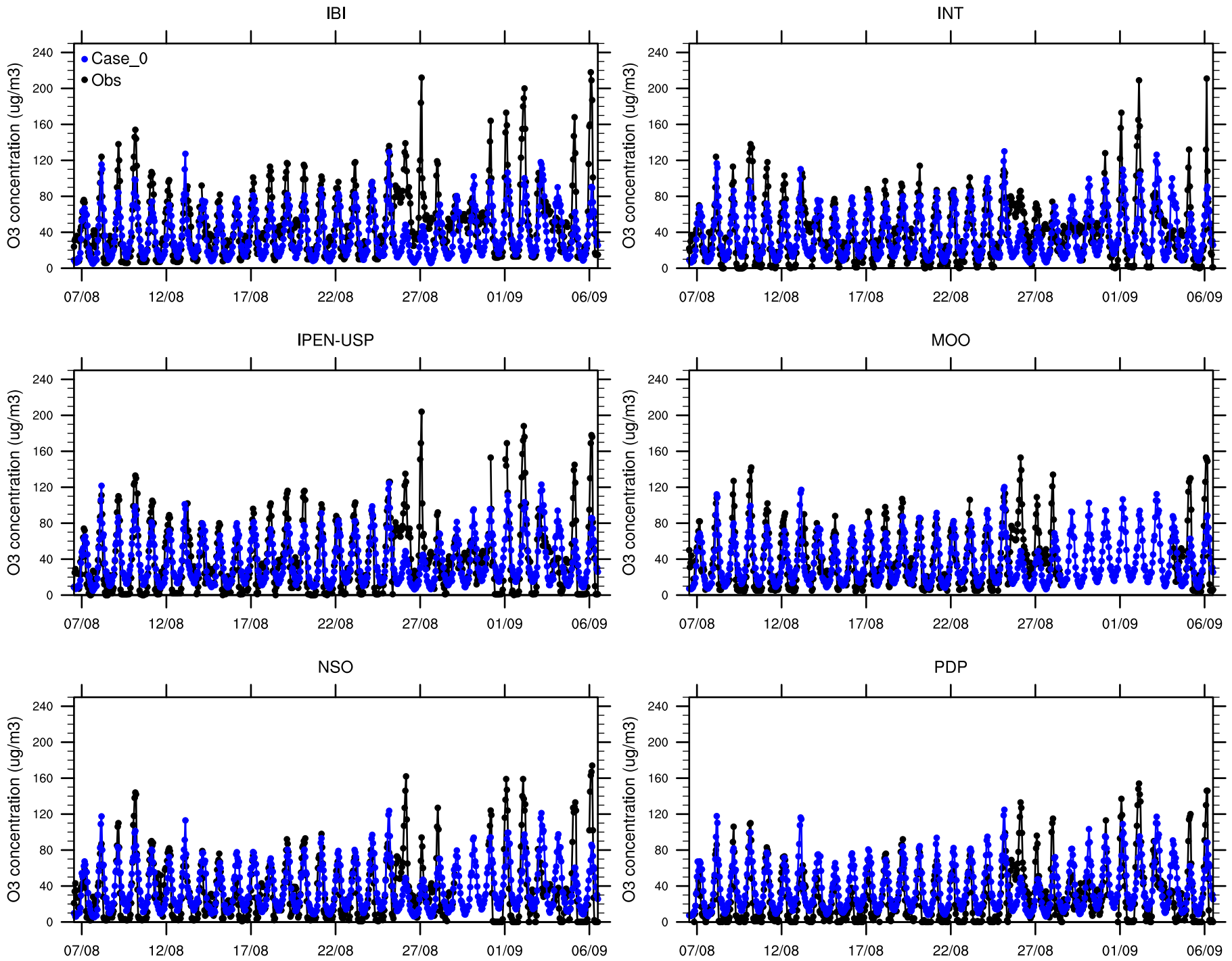
IBI
INT
IPEN-USP
MOO
NSO
PDP
Case_0
Obs
O3 concentration (ug/m3)
0
40
80
120
160
200
240
07/08
12/08
17/08
22/08
27/08
01/09
06/09

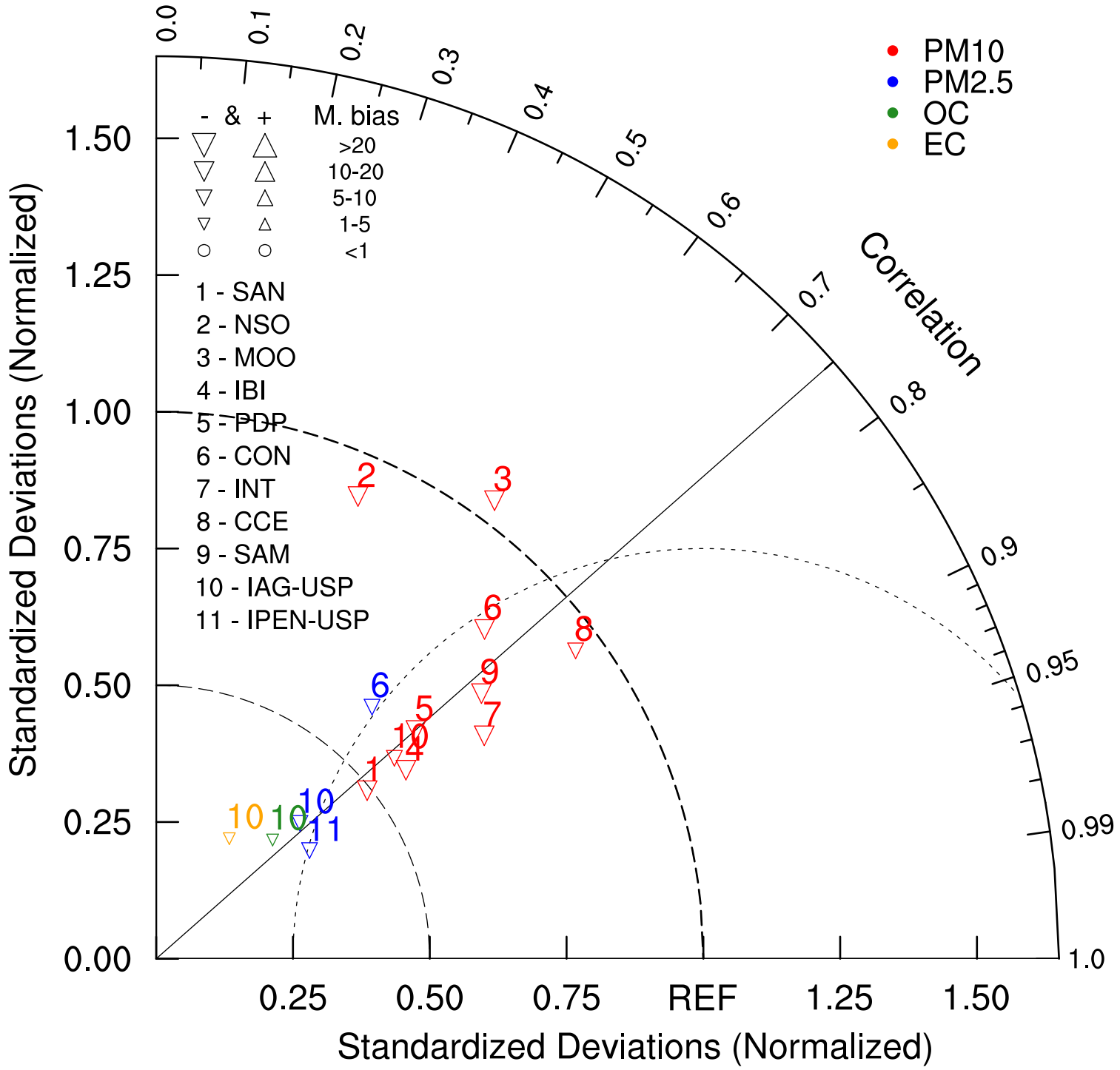
PM10
PM2.5
OC
EC
- & +
M. bias
>20
10-20
5-10
1-5
<1
1 - SAN
2 - NSO
3 - MOO
4 - IBI
5 - PDP
6 - CON
7 - INT
8 - CCE
9 - SAM
10 - IAG-USP
11 - IPEN-USP
Correlation
0.0
0.1
0.2
0.3
0.4
0.5
0.6
0.7
0.8
0.9
0.95
0.99
1.0
1.50
1.25
1.00
0.75
0.50
0.25
0.00
0.25
0.50
0.75
REF
1.25
1.50
Standardized Deviations (Normalized)
Standardized Deviations (Normalized)

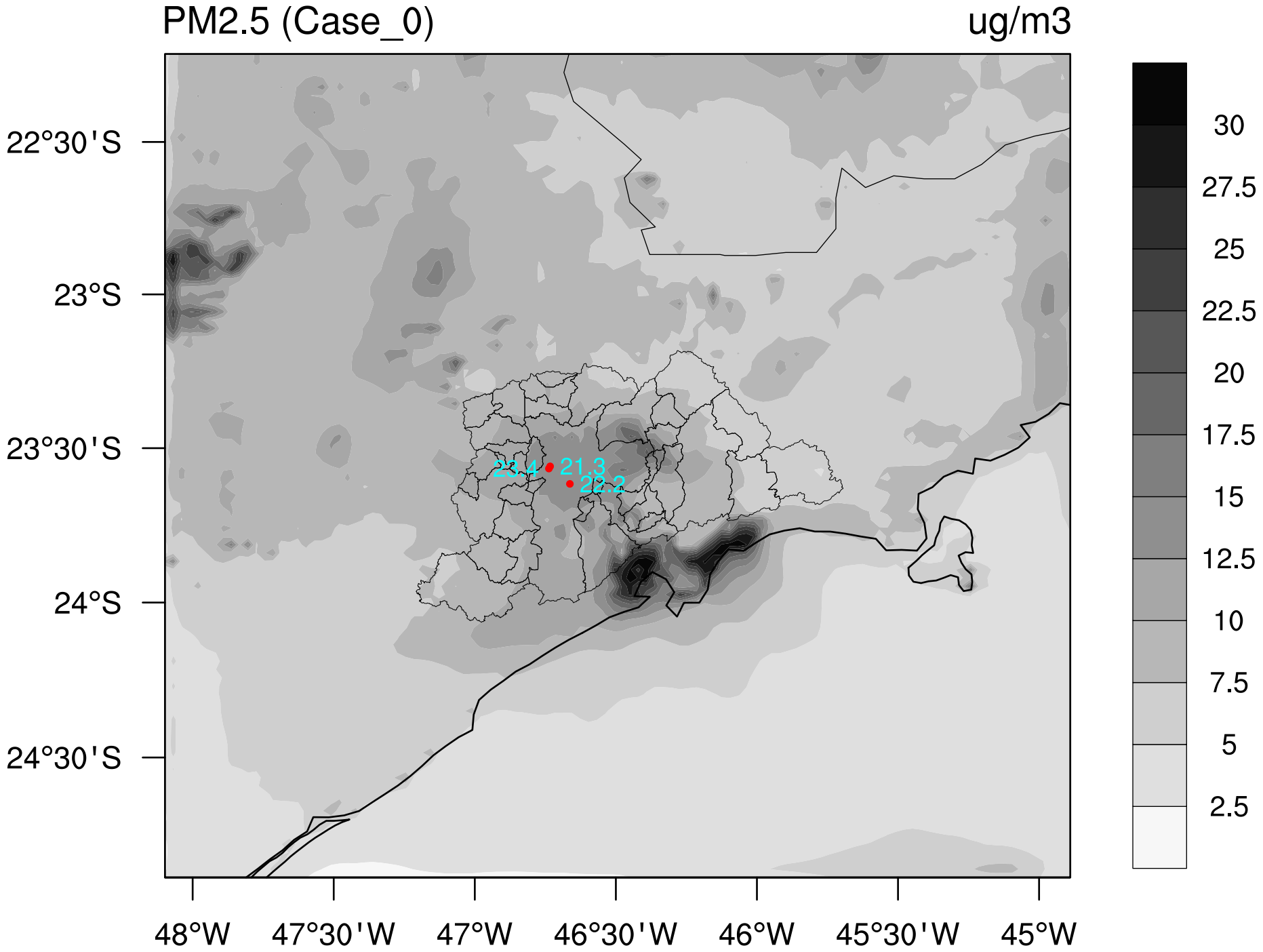
PM2.5 (Case_0)
ug/m3
22°30'S
23°S
23°30'S
24°S
24°30'S
48°W
47°30'W
47°W
46°30'W
46°W
45°30'W
45°W
23.4
21.3
22.2
30
27.5
25
22.5
20
17.5
15
12.5
10
7.5
5
2.5

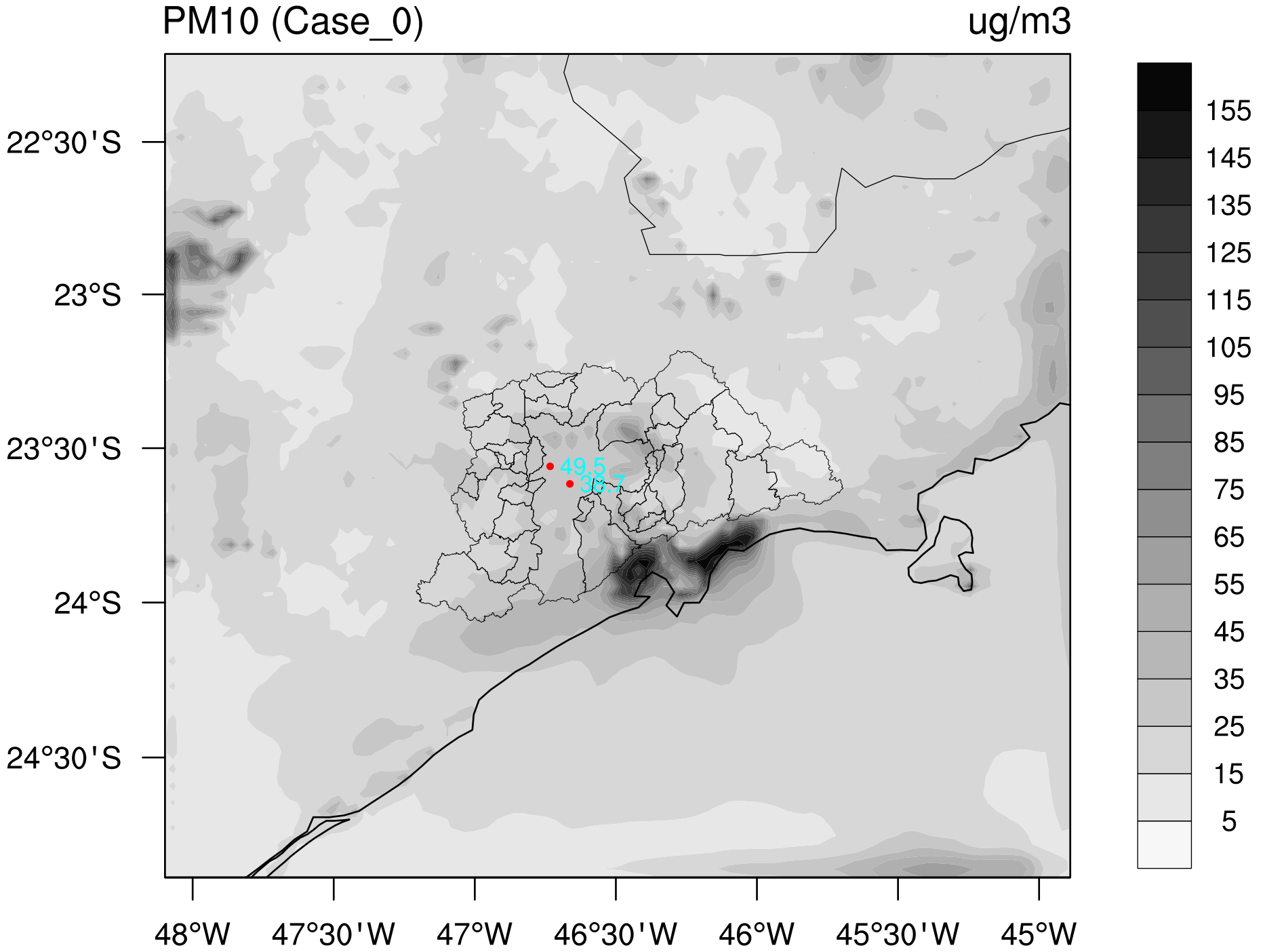
PM10 (Case_0)
ug/m3
22°30'S
23°S
23°30'S
24°S
24°30'S
48°W
47°30'W
47°W
46°30'W
46°W
45°30'W
45°W
49.5
38.7
155
145
135
125
115
105
95
85
75
65
55
45
35
25
15
5

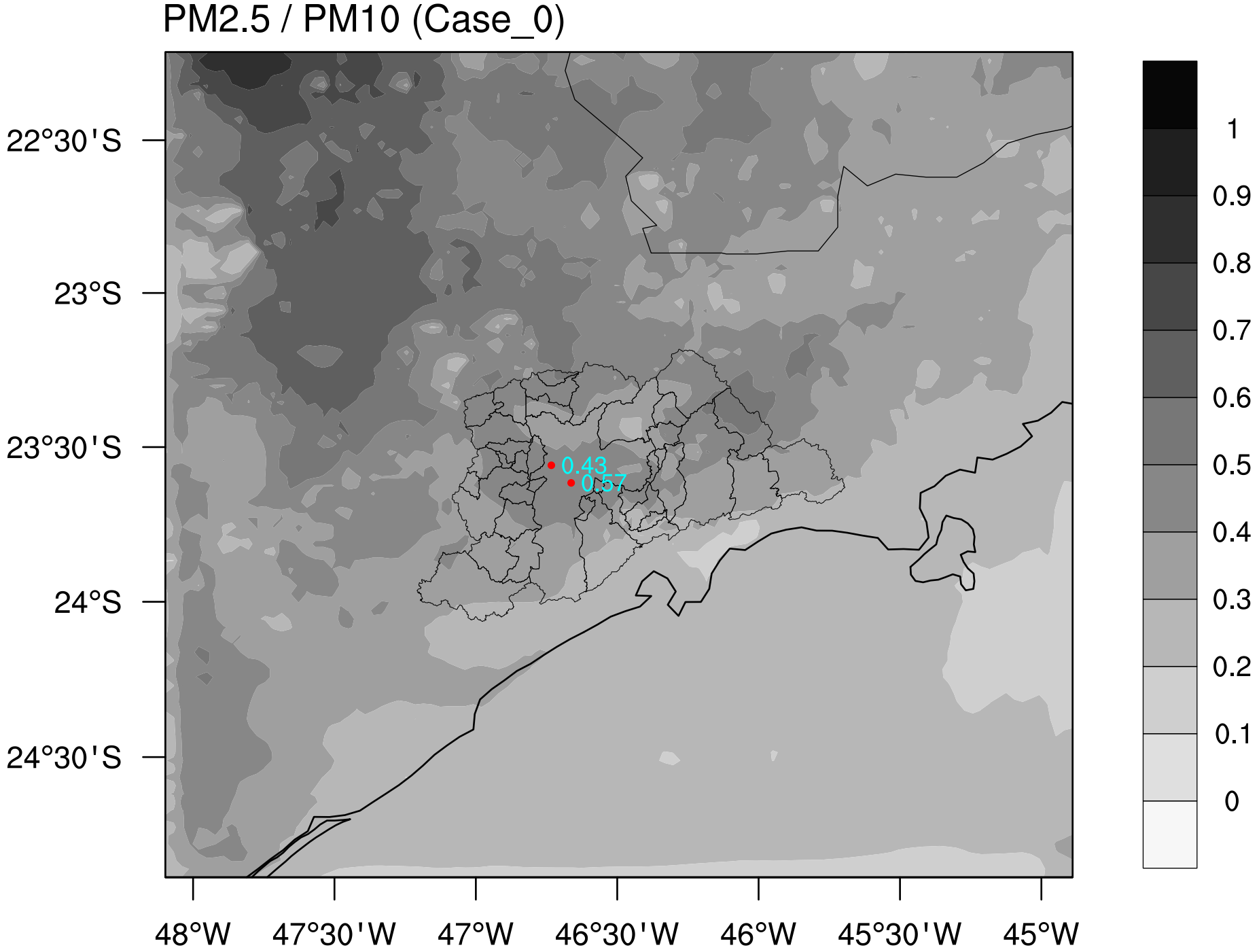
PM2.5 / PM10 (Case_0)
22°30'S
23°S
23°30'S
24°S
24°30'S
48°W
47°30'W
47°W
46°30'W
46°W
45°30'W
45°W
0.43
0.57
1
0.9
0.8
0.7
0.6
0.5
0.4
0.3
0.2
0.1
0

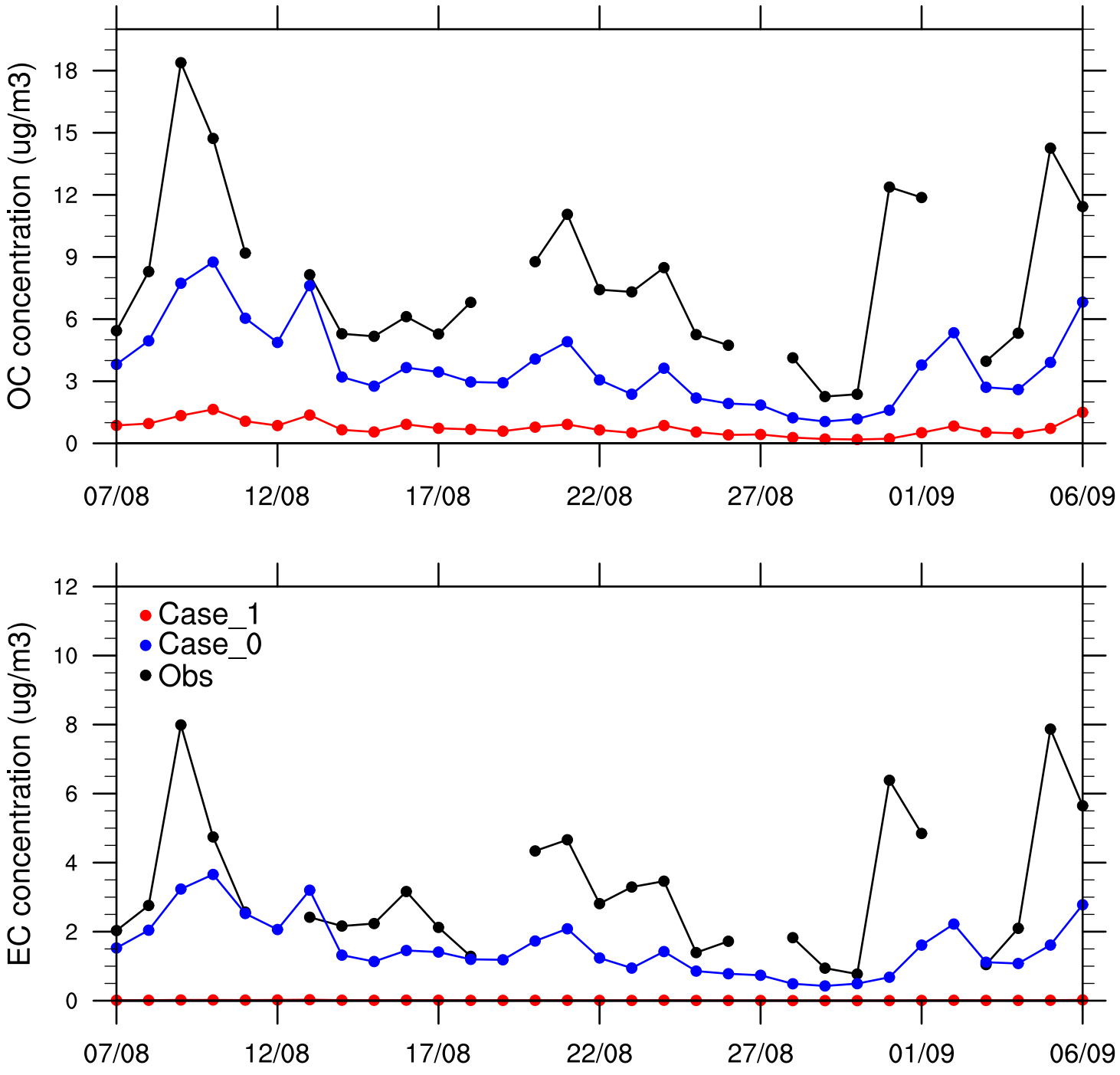
OC concentration (ug/m3)
18
15
12
9
6
3
0
07/08
12/08
17/08
22/08
27/08
01/09
06/09
EC concentration (ug/m3)
12
10
8
6
4
2
0
Case_1
Case_0
Obs
07/08
12/08
17/08
22/08
27/08
01/09
06/09

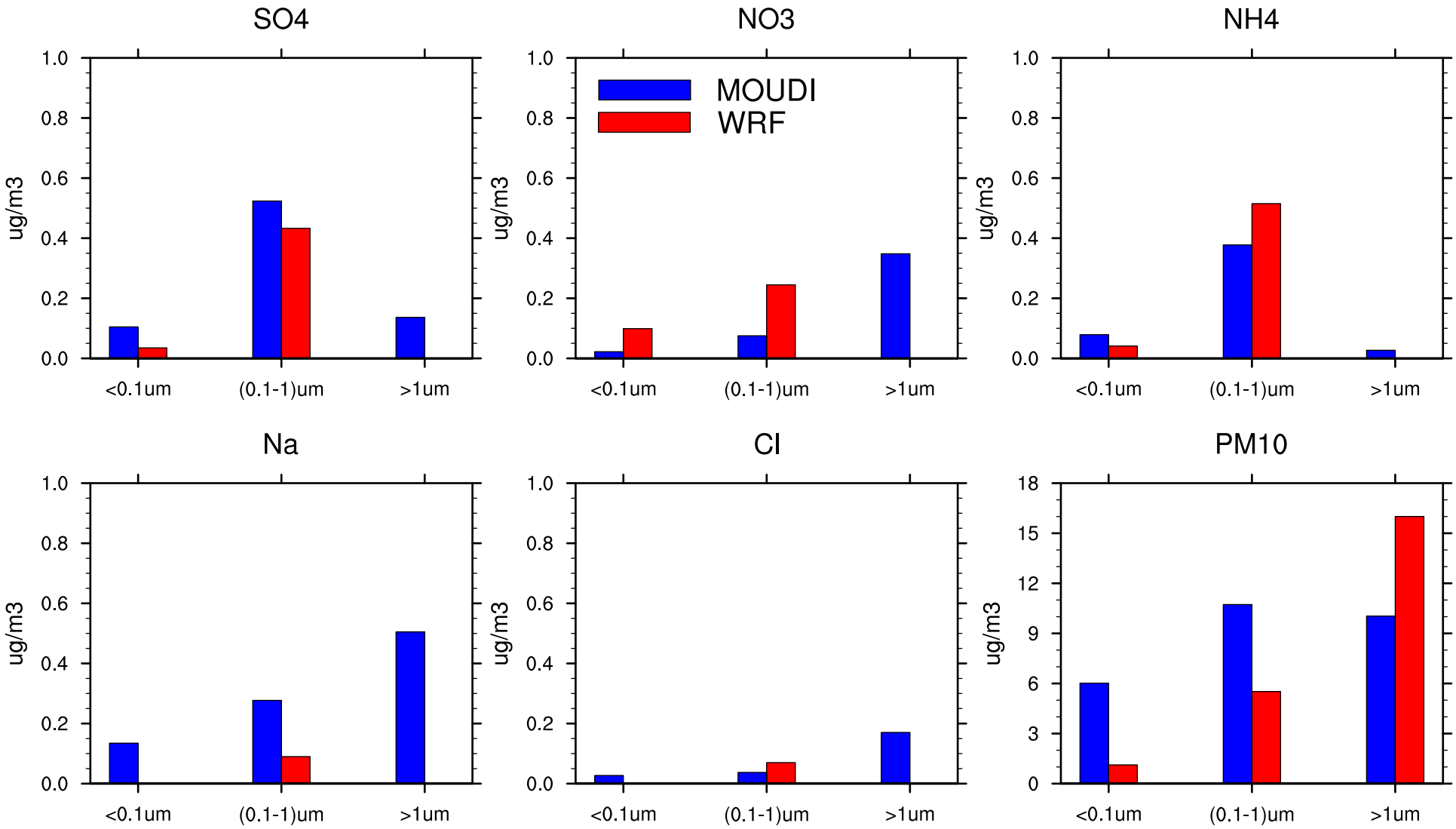
SO4
NO3
NH4
Na
Cl
PM10
MOUDI
WRF
ug/m3
<0.1um
(0.1-1)um
>1um
0.0
0.2
0.4
0.6
0.8
1.0
0
3
6
9
12
15
18

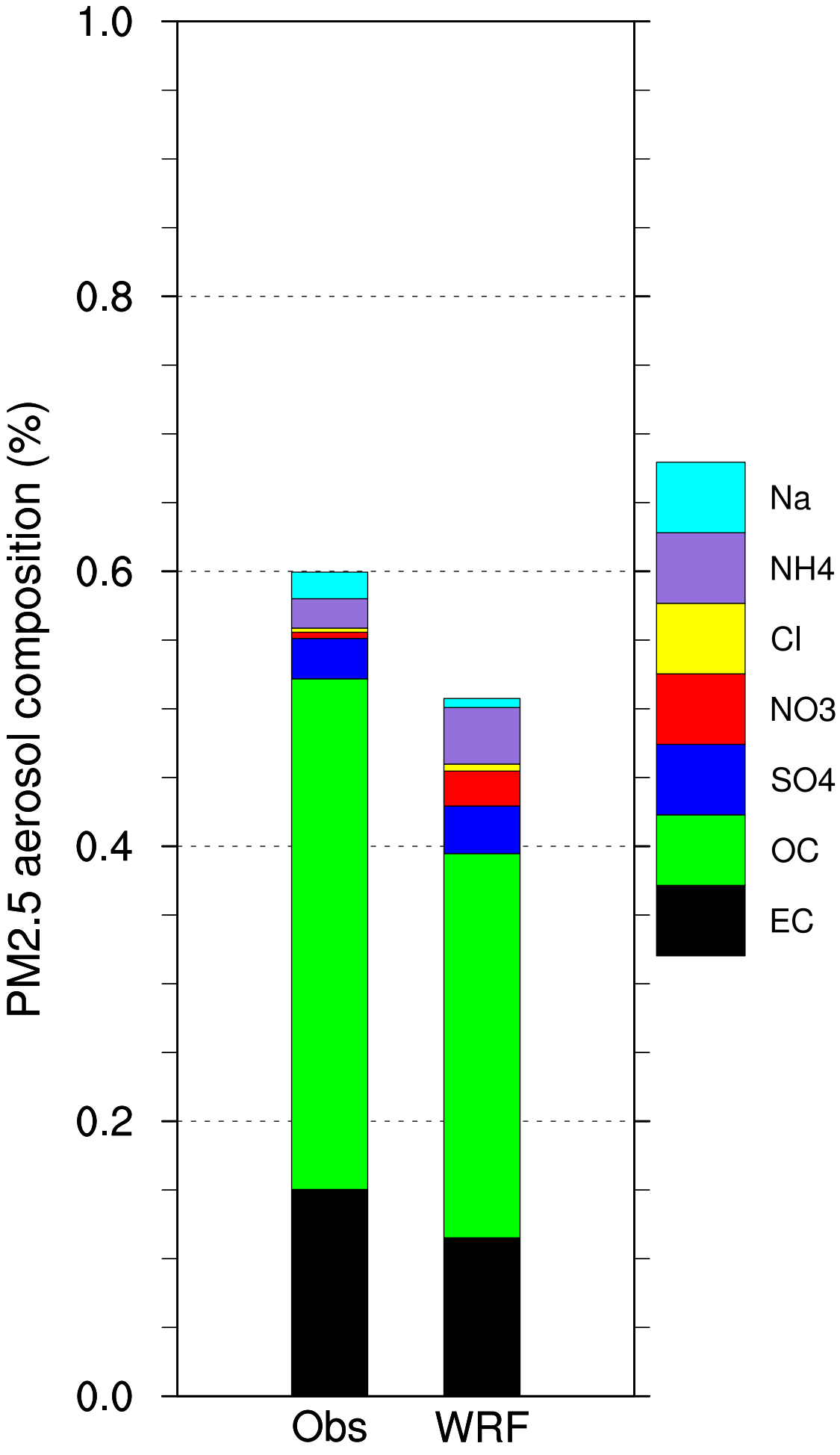
1.0
0.8
0.6
0.4
0.2
0.0
PM2.5 aerosol composition (%)
Obs
WRF
Na
NH4
Cl
NO3
SO4
OC
EC

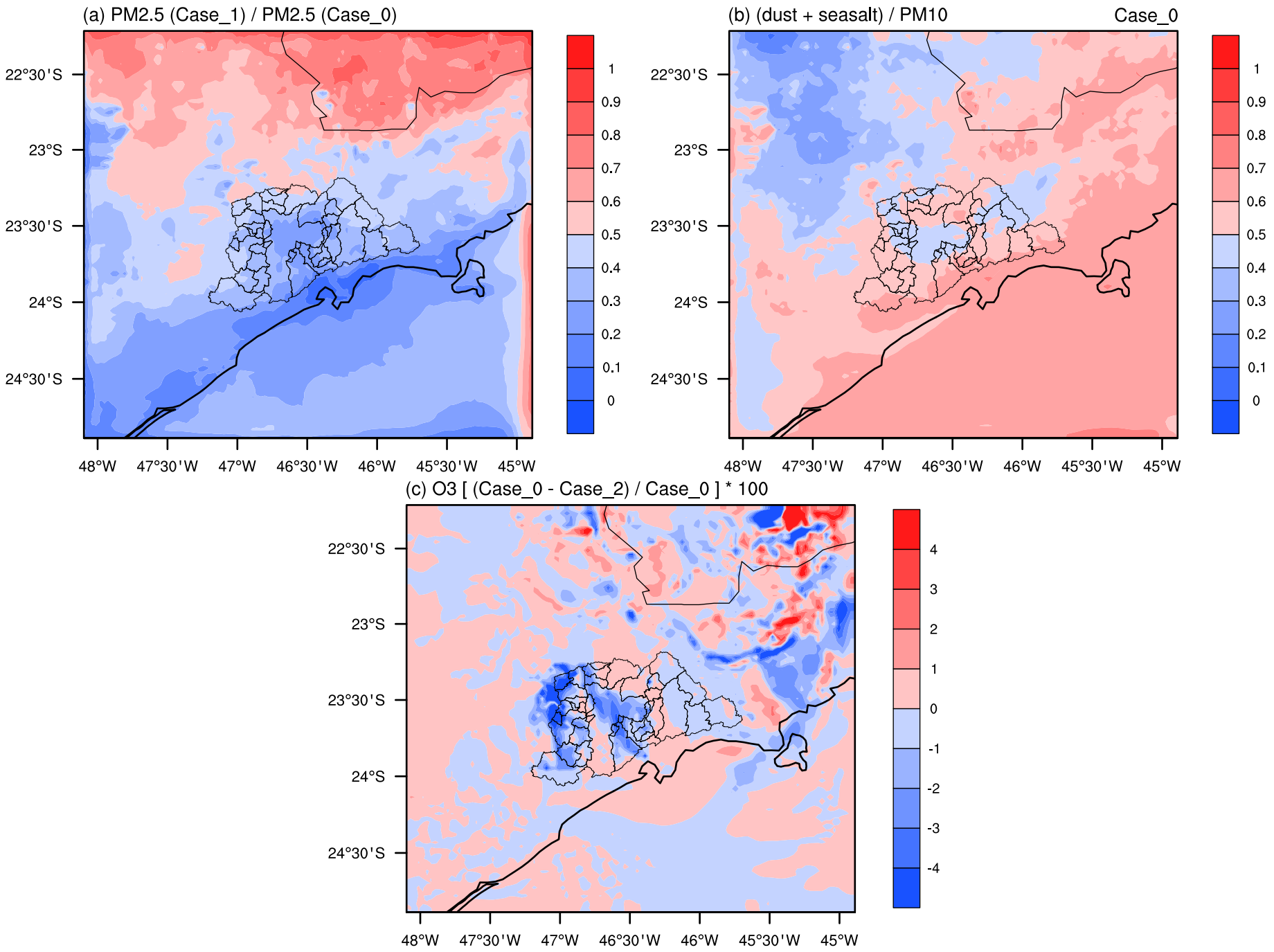
(a) PM2.5 (Case_1) / PM2.5 (Case_0)
(b) (dust + seasalt) / PM10
Case_0
(c) O3 [(Case_0 - Case_2) / Case_0] * 100
22°30'S
23°S
23°30'S
24°S
24°30'S
48°W
47°30'W
47°W
46°30'W
46°W
45°30'W
45°W
1
0.9
0.8
0.7
0.6
0.5
0.4
0.3
0.2
0.1
0
4
3
2
1
0
-1
-2
-3
-4